Characteristics of the Atlantic Storm-Track Eddy Activity and Its Relation with the North Atlantic Oscillation

G. Rivière

Atmospheric and Oceanic Sciences Program, Princeton University, Princeton, New Jersey

I. Orlanski

NOAA/Geophysical Fluid Dynamics Laboratory, Princeton University, Princeton, New Jersey

ABSTRACT

This study focuses on feedbacks of the high-frequency eddy activity onto the quasi-stationary circulation, particularly with regard to the North Atlantic Oscillation (NAO). The methodology consists of analyzing NCEP–NCAR reanalysis data and sensitivity runs from a high-resolution nonhydrostatic regional model. Consistent with recent studies, results show that the jet displacement characteristic of the NAO phenomenon depends strongly on the dynamics of the synoptic-scale waves and the way they break. Positive and negative phases of the NAO are closely related to anticyclonic and cyclonic wave breaking, respectively. Indeed, the high-frequency momentum flux whose sign is directly related to the type of wave breaking is correlated with the NAO index over the Atlantic. The peak of the momentum flux signal precedes that of the NAO by a few days suggesting that wave breaking is triggering NAO events. Two examples illustrate the significant impact of single storms, in particular those occurring in the east coast of the United States. The wave breaking at the end of their life cycle can suddenly change the NAO index in few days, and as the return to equilibrium takes generally a longer time, it can even affect the sign of the NAO during an entire month.

An important issue determining the NAO phase is related to upstream effects. By considering a domain extending from the eastern Pacific to western Europe and by forcing the regional model with real data at the western boundary, sensitivity runs show that the right sign of the NAO index can be recovered. It indicates that waves coming from the eastern Pacific are crucial for determining the NAO phase. According to their spatial scales and frequencies when they reach the Atlantic domain, they can break one way or another and push the Atlantic jet equatorward or poleward. Synoptic waves with periods between 5 and 12 days break anticyclonically whereas those with periods between 2 and 5 days break both anticyclonically and cyclonically with a predominance for cyclonic wave breaking. Another crucial factor concerns surface effects. Cyclonic wave breaking in the upper levels is strongly connected with an explosive cyclonic development at the surface accompanied by strong surface moisture fluxes whereas such an explosive growth is not present in the anticyclonic wave breaking case. Finally, it is proposed that these results are not only useful for explaining the intraseasonal variations of the NAO but would serve also as a basis for understanding its interannual and interdecadal variations.

1. Introduction

The North Atlantic Oscillation (NAO) phenomenon, which is the dominant mode of atmospheric circulation variability over the North Atlantic domain, is noticeable over a wide range of time scales. One of its well-known variations is the decadal trend that happened during the second half of the twentieth century toward a particular phase of the NAO, called the positive phase (Hurrell 1995) and that changed the climate of many areas over the Atlantic domain. The occurrence of this remarkable trend may explain the fact that a stronger emphasis in the research community has been

Corresponding author address: Gwendal Rivière, Météo-France, CNRM/GMAP/RECYF, 42 av Coriolis, 31057 Toulouse CEDEX, France.
E-mail: gwendal.riviere@meteo.fr

made to study interdecadal and interannual fluctuations of the NAO by analyzing, for example, the impacts of low-frequency external forcings such as the ocean (e.g., Rodwell et al. 1999) or the greenhouse-gas concentrations (e.g., Shindell et al. 1999). Note however that this decadal trend has reversed over the past several years and seems difficult to link with global warming (Cohen and Barlow 2005; Overland and Wang 2005).

Few other studies have recently focused on shorter time scales of the NAO and have underlined the importance of its intraseasonal variations. Feldstein (2000) has shown that the NAO as well as the Pacific–North American (PNA) teleconnections can be viewed as being stochastic processes with an *e*-folding time scale of around one week. Consistent with the previous paper, Feldstein (2003) revealed that the duration of an NAO anomaly was typically two weeks and that high-frequency eddies with periods less than 10 days are crucial in driving the NAO growth. The importance of synoptic eddies for the NAO also has been emphasized by Vallis et al. (2004) who presented a simple barotropic model of the NAO and annular modes and demonstrated that such teleconnections can be produced by stochastic stirring that mimics baroclinic eddy development. Finally, very recently, Benedict et al. (2004, hereafter B04) and Franzke et al. (2004, hereafter F04) clarified the role played by high-frequency synoptic-scale waves by showing that their breaking form the physical entity of the NAO. More precisely, anticyclonic wave breaking accompanies positive phases of the NAO while cyclonic wave breaking is linked with the formation of negative phases.

The NAO phenomenon is characterized by a meridional displacement of the upper tropospheric jet where positive and negative phases correspond respectively to a jet located further to the north and further to the south than usual. The above results of B04 and F04 are therefore consistent with other previous studies linking wave breaking processes with the jet displacement (see Thorncroft et al. 1993; Lee and Feldstein 1996; Orlanski 2003). The initial results of Simmons and Hoskins (1980), Thorncroft et al. (1993, hereafter T93) reveals that there are two distinct types of baroclinic-wave life cycles. One life cycle (LC1) ends by breaking anticyclonically, which means that the waves are elongated along the southwest–northeast (SW–NE) direction and is accompanied by a poleward shift of the jet. The other types of waves (LC2) finish their life cycle by breaking cyclonically, that is, by being northwest–southeast (NW–SE) tilted and associated with an equatorward displacement of the jet. To determine these two distinct behaviors (LC1 and LC2), T93 used two different initial jets that differed only from their barotropic component; the jet leading to LC2 had a stronger cyclonic shear than that leading to LC1. Lee and Feldstein (1996) found these two types of wave breaking in an aqua-planet general circulation model and related also the type of wave breaking to the strength of the meridional shear in the upper troposphere.

Orlanski (2003, hereafter Or03), recovered the two same life cycles in a shallow water model but, in contrast with the two previous studies, did not underline the role of the barotropic component of the basic state in the control of wave breaking. His results place emphasis on a vortex interaction mechanism that can be controlled by the intensity of the low-level baroclinicity or the moisture fluxes. For weak intensities, because of the effective beta effect upper-level waves usually break anticyclonically that makes the jet move poleward. For moderate intensities, the areas of anticyclones become bigger than those of cyclones. In this case, anticyclones dominate over cyclones and produce a circulation that stretches the cyclones along the SW–NE direction. This creates globally anticyclonic wave breaking and the jet is still shifted northward. As the intensity of the forcing increases, cyclones can be more intense than anticyclones but the latter still dominate because of their large area and more violent anticyclonic wave breaking occurs. However for stronger intensities, it comes to a point in which anticyclonic vorticities cannot decrease less than $-f$ (Coriolis parameter), whereas cyclonic vorticities do not have such a limit. This will render the cyclones so intense that they will dominate and will stretch the anticyclones along a NW–SE direction. This configuration creates cyclonic wave breaking and pushes the jet equatorward. Orlanski (2005, hereafter Or05), has applied the previous theoretical results to understand the PNA teleconnection. It was shown in particular that anticyclonic (cyclonic) wave breaking creates a ridge (trough) in the eastern Pacific and that the type of breaking is in part controlled by SST anomalies created by ENSO because of their direct influence on the low-level baroclinicity.

The papers mentioned in the previous paragraphs agree on the close relationship between wave breaking and the meridional displacement of the upper tropospheric jet and strongly support the idea that wave breaking is responsible for the jet motion. Furthermore, it suggests that studies on wave breaking can help to improve our understanding of the NAO and PNA teleconnections. However, arguments to explain the reasons why waves break one way or another do not go in the same direction and seem to raise open questions.

Our study is in the same vein as those of B04 and F04. Our focus is on the synoptic eddy feedback onto the

large-scale atmospheric circulation associated with the NAO phenomenon and the role of wave breaking. The questions we will address are the following:

- How can we relate eddy momentum fluxes, wave breaking, and the NAO?
- How can we quantify wave breaking?
- What are the properties of the waves; that is, what are their spatial and temporal scales and energy that will make them break one way or another?

B04 was an observational study showing evidence that anticyclonic (cyclonic) wave breaking occurs during positive (negative) phases of the NAO but most of the previous questions were not discussed. By analyzing initial value problems in a primitive equation model, F04 investigated the features that control the type of wave breaking and found a strong dependence on the latitudinal positions of the synoptic waves coming from the Pacific. Our study will differ from the previous one by the methodology used as well as by the underlined factors that influence wave breaking.

The study is presented as follows. Section 2 describes our methodology, which is based on the National Centers for Environmental Prediction–National Center for Atmospheric Research (NCEP–NCAR) reanalysis dataset and on a high-resolution nonhydrostatic model. Section 3 shows the effect of waves coming from the eastern Pacific by comparing some simulations to the reanalysis. Section 4 is dedicated to prove the close relation between wave breaking and the NAO on monthly time scales as well as to quantify wave breaking. The difference between cyclonic and anticyclonic wave breaking processes (CWB and AWB, respectively) is investigated in section 5. Section 6 focuses on longer time scales, on the interannual and interdecadal variations of the NAO. Finally, conclusions are provided in section 7.

2. Methodology

a. Reanalysis

The dataset used in this study is the twice-daily NCEP–NCAR reanalysis (at 0000 and 1200 UTC) on a $2.5° \times 2.5°$ grid from 1950 to 1999. All the results shown hereafter concern only the winter season from December to February since the NAO has a stronger variability during this period. A daily average of the dataset at 0000 UTC and 1200 UTC is performed for most of the figures apart from some specific figures where the twice-daily dataset is used directly without averaging (where appropriate, specifics are noted in the text). To identify the role played by synoptic eddies in the NAO

phenomenon, a 31-point Lanczos filter with a 12-day cutoff is applied to the daily average to separate the high-frequency signal corresponding to the synoptic eddies from the other part of the flow. More information about this high-pass filter is given in appendix A. The high-frequency signal obtained has periods between 2 and 12 days and therefore includes all frequencies of the synoptic waves. But for reasons detailed later, we also consider two distinct ranges of frequencies inside this synoptic signal, an intermediate-frequency range (periods between 5 and 12 days) and a very-high-frequency range (periods between 2 and 5 days) by using the 5-day filter described in appendix A.

In our study, we use a monthly NAO index computed by the Climate Diagnostics Center of the National Oceanic and Atmospheric Administration (available online at http://www.cdc.noaa.gov/ClimateIndices/) and based on the rotated principal component technique as in Barnston and Livezey (1987). A daily NAO index is also defined by regressing the climatological anomaly of the daily average geopotential field at 300 hPa against the dipole pattern of the NAO over the Atlantic domain (20°–90°N, 100°W–40°E). This dipole pattern was previously obtained from the monthly dataset by time-regressing the monthly geopotential field on the monthly NAO index. This approach avoids the computation of an EOF for a daily time series without significantly changing the results [indeed, the EOF for a daily dataset is very close to that computed for a monthly one as shown by Feldstein (2000)]. We also verified that the variations of the previously defined daily NAO index were similar to those shown in Fig. 1 of B04.

b. Model

The other part of our results is based on the integration of a high-resolution nonhydrostatic ZETAC model developed by S. Garner at the Geophysical Fluid Dynamics Laboratory (GFDL; more information available at http://www.gfdl.noaa.gov/~stg/). It has been already described and used over the Pacific domain to study the PNA teleconnection by Or05. It shares physics schemes and packages with other atmospheric models of the GFDL's Flexible Modeling System. The moisture scheme is an explicit moist convection with a Kessler microphysics parameterization and the vertical coordinate is a terrain-following coordinate. ZETAC can be used as a regional or global atmospheric model; in the present case, the simulation area goes from 150°W to 10°E and 10°S to 85°N and covers the northeastern Pacific as well as the entire North Atlantic. The regional component model has open lateral boundaries (see appendix of Or05 for more details) and the horizontal resolution in our simulations
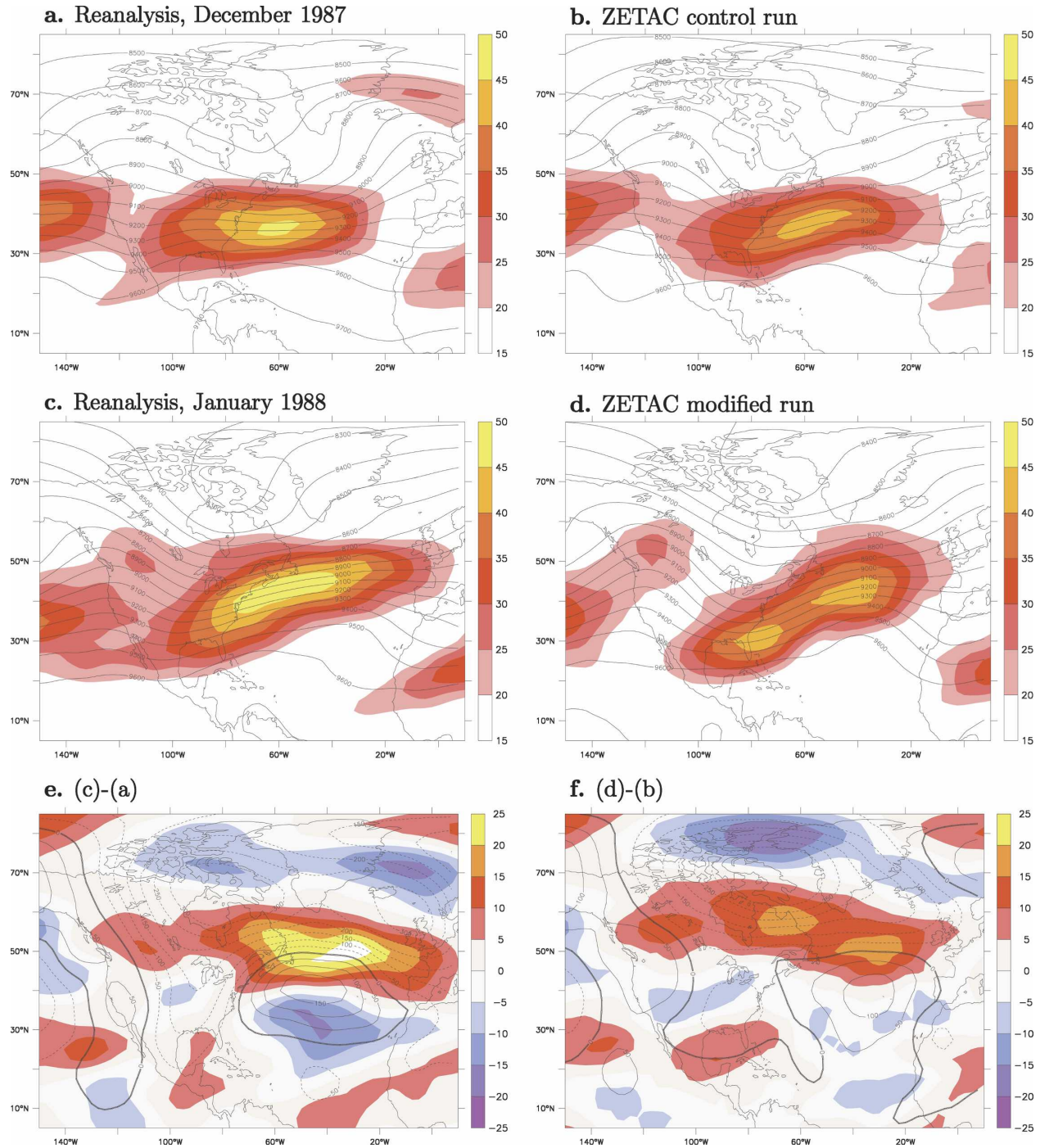
FIG. 1. Monthly averages of geopotential height (black contours, in m) and zonal wind (color shadings, in m s^{-1}) at 300 hPa. The left column corresponds to NCEP reanalysis results: averages during (a) December 1987 and (c) January 1988, and (e) the difference between (c) and (a). The right column corresponds to ZETAC runs: (b) the average for the control run; i.e., with all the forcings coming from December 1987, and (d) the average for the modified run (the forcing at the western boundary corresponds to January 1988), and (f) the difference between (d) and (b).

is around 50 km. It is forced by a prescribed SST over the surface of the ocean and is relaxed toward a time-dependent flow at the western boundary. The latter two forcings were already used in Or05 but here are pre-

scribed with real data (NCEP–NCAR reanalysis dataset) rather than the artificial seeding used in Or05. The forcing at the western boundary is useful to represent the westerlies that are present in the eastern Pa-
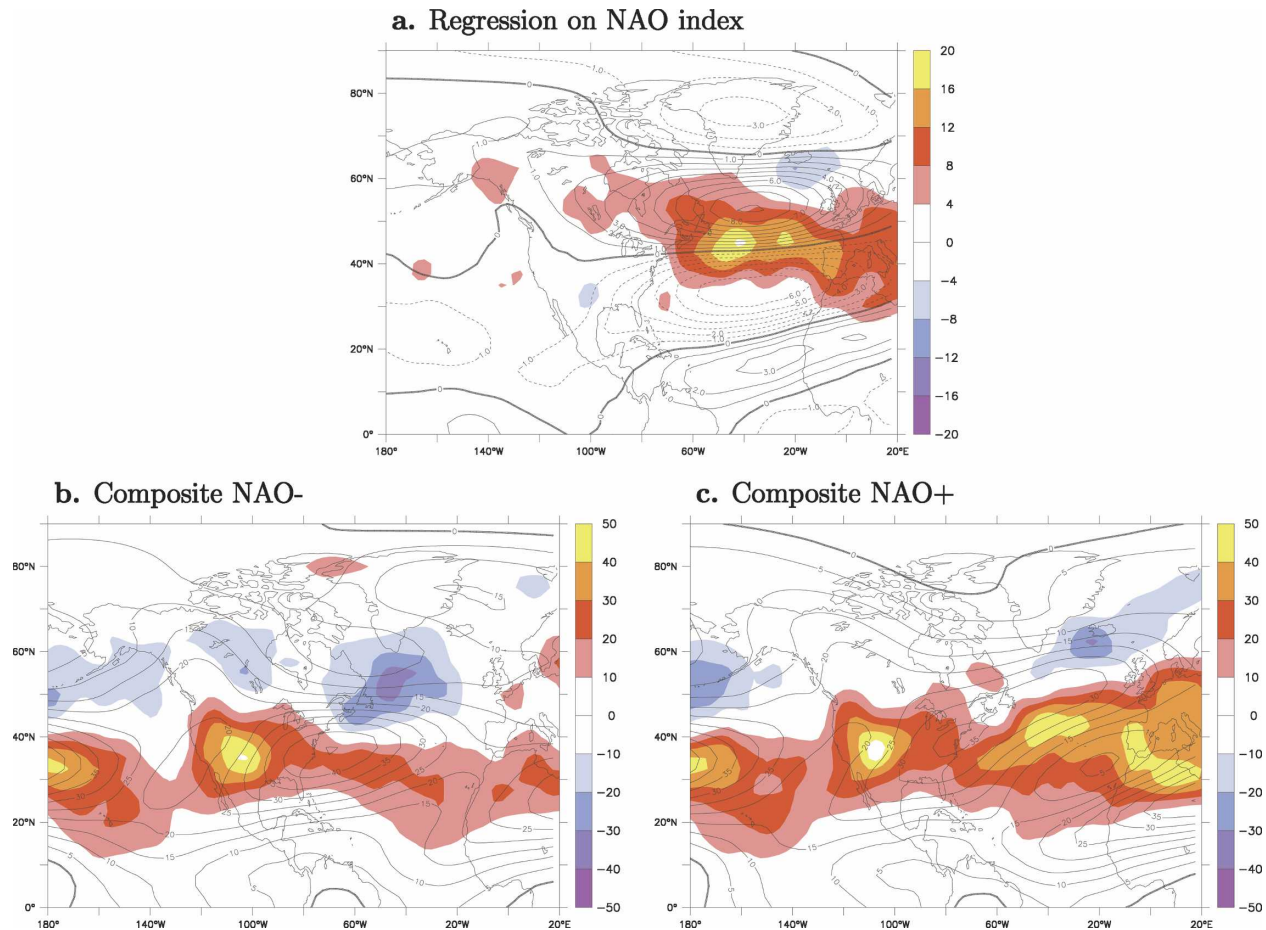
a. Regression on NAO index

b. Composite NAO-   **c.** Composite NAO+

FIG. 2. (a) Regression on the monthly NAO index of the zonal wind (black contours, contour interval is 1 m s^{-1}) and the high-frequency momentum fluxes (shadings, in m^2 s^{-2}) for winter months December–February (DJF) from 1950 to 1999. (b), (c) The monthly mean composites of the zonal wind (black contours, contour interval is 5 m s^{-1}, isotachs less than 0 m s^{-1} omitted) and the momentum fluxes (color shadings, in m^2 s^{-2}) for values of the NAO index below -1 and above 1, respectively (1 being the standard deviation), and for the same season and period as the regression.

cific as well as the waves that propagate eastward and can influence the atmospheric circulation inside the Atlantic domain. One major interest of this approach is that we do not prescribe a priori a basic state inside the domain and the model is free to develop its own large-scale circulation. Initial conditions are also coming from the same reanalysis database. To conclude, three different parameters coming from the reanalysis database are included in our simulations (SST, the nudge at the western boundary, and the initial conditions), and our sensitivity runs consist of modifying these three different parameters.

3. Local versus upstream effects setting the NAO

Numerous studies have investigated the impact of Atlantic SSTs on the NAO as discussed in the review of Rodwell (2003). Others have already focused on non-

local oceanic effects such as those created by SST anomalies in the tropical Pacific. But curiously, nonlocal effects coming from the atmospheric circulation itself have not received much attention apart from the work of F04. Their results show evidence of upstream tropospheric effects on the NAO by adopting an initial value problem with a primitive equation model. By adding synoptic perturbations in the Pacific to different basic states, the authors demonstrate that their model is able to reproduce both phases of the NAO; the essential ingredient determining the NAO phase is the initial latitudinal position of the perturbations. Our aim in this section is to present other upstream effects setting the NAO, different from the previous ones, but coming also from the tropospheric flow in the eastern Pacific.

Two consecutive months were studied, December 1987 and January 1988 (hereafter D87 and J88), that are of particular interest since they correspond to two
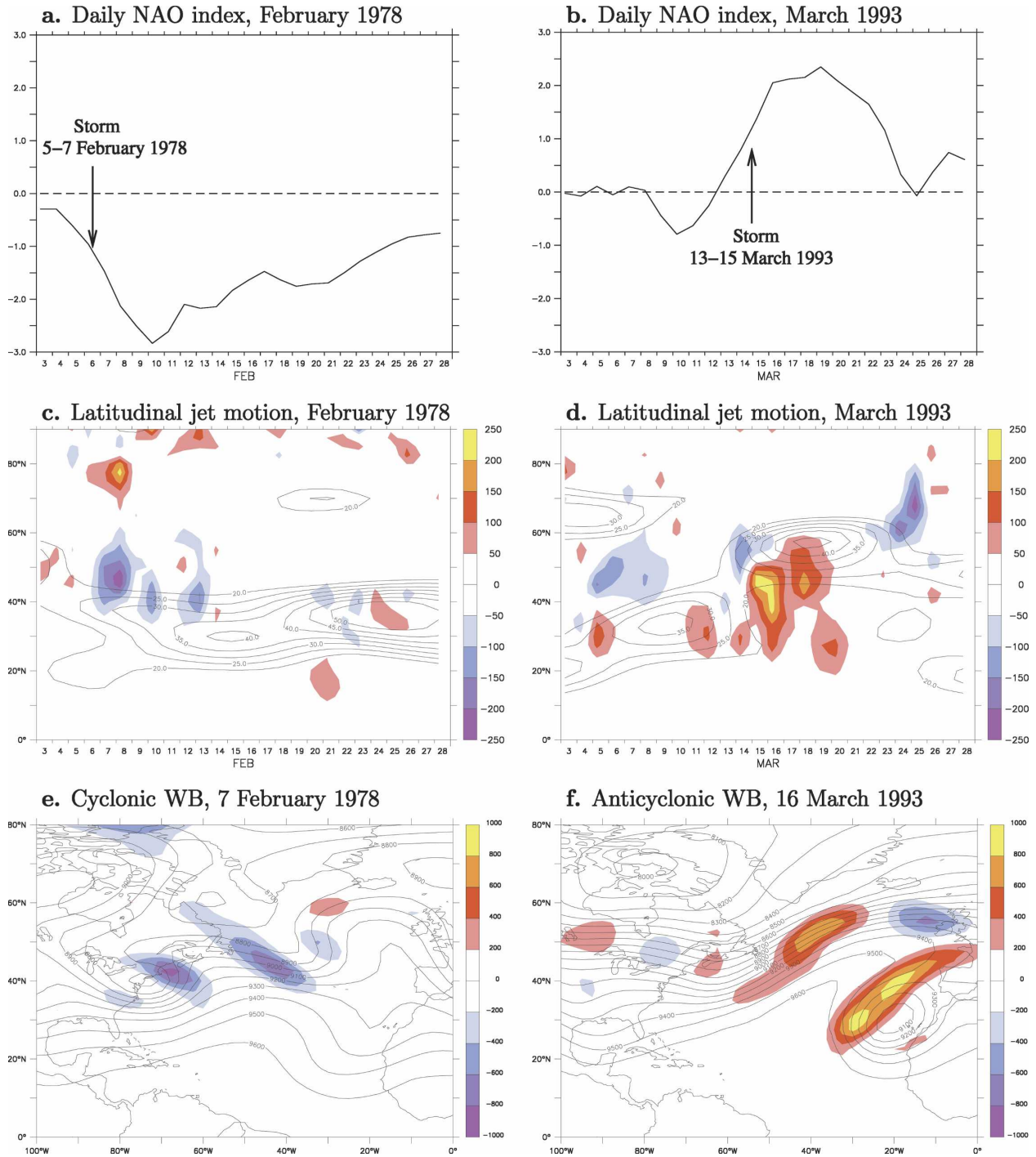
FIG. 3. Effect of two single storms (5–7 Feb 1978) and (13–15 Mar 1993) on NAO. The negative and positive NAO events of February 1978 and March 1993 are triggered by the two respective storms; daily NAO indexes for the months of (a) February 1978 and (b) March 1993. (c), (d) Time–latitude plots of the low-frequency zonal wind (black contours, contour interval is 5 m s^{-1}, isotachs less than 20 m s^{-1} omitted) and of the high-frequency momentum fluxes (color shadings, in m^2 s^{-2}) (the longitude average is done between 60° and 0°W) for February 1978 and March 1993, respectively. (e), (f) Geopotential height (black contours, contour interval is 100 m) and the momentum fluxes (color shadings, in m^2 s^{-2}) at 300 hPa, respectively, for 7 Feb 1978 and 16 Mar 1993.

opposite phases of the NAO. D87 was a negative NAO month whereas J88 was a positive month. This difference can be viewed from Figs. 1a,c,e. For example, the upper-tropospheric Atlantic jet in J88 (Fig. 1c) is located more northward than that in D87 (Fig. 1a) and extends more eastward too. This typifies the difference between the negative and positive NAO. Moreover, by subtracting the geopotential field of J88 from that of D87, the pattern obtained over the Atlantic domain (Fig. 1e) is characterized by a south–north dipole anomaly, also a characteristic feature of the NAO. The spatial correlation inside the Atlantic domain (20°–90°N, 100°W–10°E) between the geopotential anomaly of Fig. 1e and the geopotential NAO anomaly (obtained by regressing the monthly geopotential anomalies on the monthly NAO index defined in section 2a) is equal to 0.75. This rapid intraseasonal variation of the NAO suggests that low-frequency forcings like the ocean play a secondary role and that internal atmospheric mechanisms are more important.

A control simulation of D87 was performed as follows: averaged SSTs of D87 were used, 1 December reanalysis data served to initialize the model and the nudge at the boundaries, in particular input at the western boundary, was given by the twice-daily reanalysis dataset of D87 at that location. The forcing at the western boundary is therefore composed of the time-dependent jet in the eastern Pacific during D87 as well as of all the waves that traveled through this region during this month. The result of this control simulation is shown in Fig. 1b. The simulated Atlantic jet is quite comparable with the real jet of D87 (Fig. 1a) in terms of its location, width, and length while its intensity is slightly weaker. The result of another 30-day run called the modified run is shown in Fig. 1d. This modified run has the same environmental conditions as the control one; that is, is forced by the same SSTs and has the same initial conditions. Only the flow at the western boundary has been changed from D87 to J88. The zonal wind average of the modified run is significantly different from that of the control run and exhibits a jet located more northerly in the Atlantic domain. The difference between Figs. 1d and 1b is displayed in Fig. 1f. It exhibits a dipole anomaly in the geopotential field characteristic of the NAO that is quite similar to that shown in Fig. 1e. The spatial correlation between the geopotential anomalies of Figs. 1e,f over the Atlantic is equal to 0.82. These results demonstrate that the flow at the western boundary is crucial to determine the phase of the NAO and suggests that the waves coming from the eastern Pacific that propagate inside the Atlantic domain play an important role. A more detailed analysis is performed at the end of next section to investigate
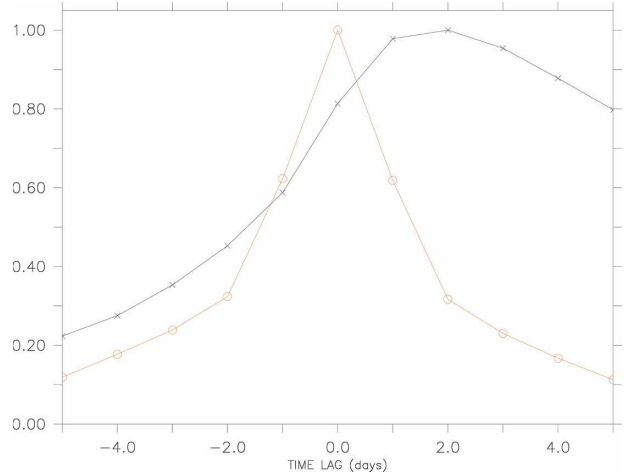

FIG. 4. Time-lag regressions based on an index that is defined as the high-frequency momentum fluxes averaged over the Atlantic (35°–55°N, 60°–0°W). The regressed variables are the daily NAO index (black curve with crosses) and the averaged momentum fluxes over the same area (red curve with circles) during winter months (DJF) from 1950 to 1999. The x axis corresponds to the different time lags while the y axis is the regression divided by its maximum.

behavioral differences between the two months. Note finally that we have performed another two runs (not shown here) with the initial conditions of J88 and the SSTs of J88 and by using the western boundaries of J88 and D87 that lead to the same conclusions.

4. NAO and wave breaking on monthly time scales

By neglecting dissipation and vertical advection, and by approximating the Coriolis parameter by a constant value f_0, the zonal momentum equation for a non divergent flow can be written as

$$\frac{\partial}{\partial t}(\hat{u} + u') + \hat{u}\partial_x\hat{u} + \hat{v}\partial_y\hat{u} + \hat{u}\partial_x u' + \hat{v}\partial_y u' + u'\partial_x\hat{u}$$

$$+ v'\partial_y\hat{u} = f_0(\hat{v}_a + v'_a) - (u'^2)_x - (u'v')_y, \quad (1)$$

where hats and primes denote respectively the low-frequency and high-frequency parts of the flow, (u, v) are the horizontal wind components. The equation to study the eddy feedback onto the large-scale atmospheric circulation is obtained by applying the low-frequency filter to Eq. (1). The terms composed of the multiplication of low-frequency quantities by high-frequency ones; that is, $\hat{u}\partial_x u'$, $\hat{v}\partial_y u'$, $u'\partial_x\hat{u}$, and $v'\partial_y\hat{u}$ project essentially onto the high-frequency part and the equation governing the evolution of the low-frequency zonal wind can be thus approximated by
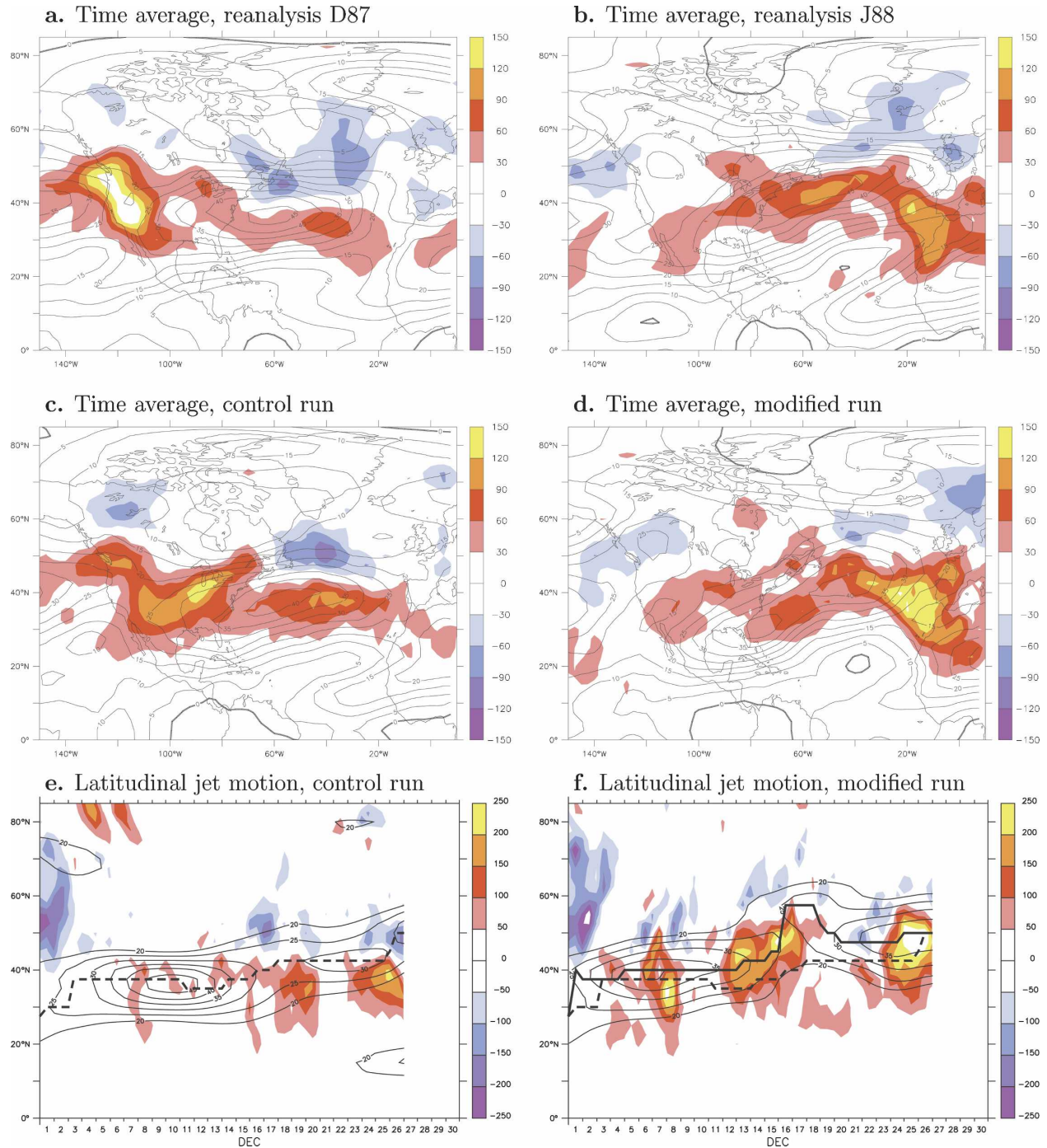
a. Time average, reanalysis D87

b. Time average, reanalysis J88

c. Time average, control run

d. Time average, modified run

e. Latitudinal jet motion, control run

f. Latitudinal jet motion, modified run

FIG. 5. (a), (b) Time averages of the zonal wind (black contours, contour interval is 5 m s^{-1}, isotachs less than 0 m s^{-1} omitted), and the high-frequency momentum fluxes (color shadings, in m^2 s^{-2}) at 300 hPa for the reanalysis of D87 and J88, respectively. (c), (d) Same as (a) and (b) but for the control and modified runs respectively. (e), (f) Time–latitude plots (longitude average done between 60°W and 10°E) of the low-frequency zonal wind (black contours, contour interval is 5 m s^{-1}, isotachs less than 20 m s^{-1} omitted) and of the high-frequency momentum fluxes (color shadings, in m^2 s^{-2}) for the control and modified runs, respectively. The dashed and solid lines in (e) and (f) correspond to the latitude of the maximum zonal wind in the control and modified runs.

$$\frac{\partial}{\partial t}\hat{u} + \hat{u}\partial_x\hat{u} + \hat{v}\partial_y\hat{u} = f_0\hat{v}_a - (\widehat{u'^2})_x - (\widehat{u'v'})_y. \quad (2)$$

Hoskins et al. (1983) and Trenberth (1986) have introduced the **E** vector that characterizes the eddy anisotropy and have shown that its divergence corresponds to the eddy feedback onto the quasi-stationary circulation. The two papers differ slightly in their definition of the **E** vector as the latter depends on the eddy terms that are included in the residual meridional circulation. In what follows, the definitions of Hoskins et al. (1983) are chosen and lead to the following expression of Eq. (2)

$$\frac{\partial}{\partial t}\hat{u} + \hat{u}\partial_x\hat{u} + \hat{v}\partial_y\hat{u} = f_0\hat{v}_a^* + \nabla \cdot \mathbf{E}, \quad (3)$$

where $\mathbf{E} \equiv (\widehat{v'^2} - \widehat{u'^2}, -\widehat{u'v'})$ and $\hat{v}_a^* \equiv \hat{v}_a - f_0^{-1}(\widehat{v'^2})_x$.

The third term on the right-hand side of (2) or equivalently the y derivative of the **E** vector in (3) involves the eddy momentum fluxes and can be easily related to wave breaking and to the meridional displacement of the jet. Indeed, when AWB occurs, eddies are tilted along the SW–NE direction which leads to positive values of the meridional eddy momentum fluxes $\widehat{u'v'}$. Farther north and south of the zone where AWB occurs, $\widehat{u'v'}$ decreases to zero, which means that $(\widehat{u'v'})_y$ is positive and negative, respectively, north and south of the $\widehat{u'v'}$ maximum. From (2), this implies that $\hat{u}$ will increase in the north and decrease in the south. In this case, the jet is pushed poleward if we suppose that the momentum fluxes maximum is located near the zonal wind maximum. A similar argument for CWB leads to the conclusion that CWB pushes the jet equatorward. This qualitative description allows us to make a bridge between wave breaking, momentum fluxes, and the jet displacement. It also can explain the results of B04 and F04 showing that anticyclonic (cyclonic) wave breaking occurs more during positive (negative) NAO when the jet goes more to the north (south).

Two regression maps based on the monthly NAO index are shown in Fig. 2a where the variables are the monthly averages of the zonal wind and the high-frequency meridional momentum fluxes in the upper troposphere (300 hPa). The high-frequency momentum fluxes were obtained by applying the 12-day high-pass filter described in appendix A to the two horizontal wind components separately and then by multiplying them together. The momentum fluxes regression map possesses a prominent positive signature over the entire Atlantic domain between 40° and 50°N, that is, where the Atlantic storm track is usually located. This proves that positive (negative) momentum fluxes happen more during a positive (negative) NAO. Note also that the
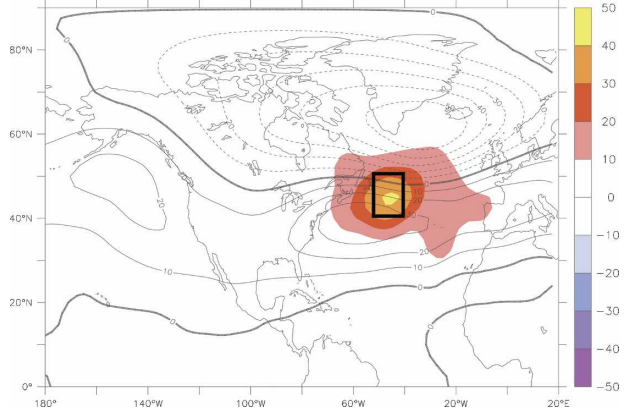

FIG. 6. Regression based on an index that is defined as the high-frequency momentum fluxes averaged over a small area in the western Atlantic (40°–50°N, 50°–40°W). The regressed variables are the geopotential height (black contours; solid and dashed lines for positive and negative values; contour interval is 10 m) and the high-frequency momentum fluxes (color shadings, in $m^2\,s^{-2}$) during winter months (DJF) from 1950 to 1999.

maxima of the regressed momentum fluxes are located exactly along the line where the regressed zonal wind is zero; above this line, the zonal wind anomalies are positive and below they are negative. This feature shows that the meridional gradient of the anomalous momentum fluxes is spatially correlated with the zonal wind fluctuations consistent with relation (2). Composites of the same two variables for negative (Fig. 2b) and positive (Fig. 2c) NAO months corroborate the previous results. For the negative NAO composite, the negative momentum fluxes are stronger in amplitude than the positive ones over the Atlantic domain whereas the reverse occurs for the positive NAO composite. The conclusion is that more CWB than AWB occurs during negative NAO months and vice versa for positive NAO months. Note that we have checked that the difference in wave breaking between the two phases of the NAO is not due to the meridional shears of the jet. For example, the anticyclonic shears of the jets shown in Figs. 2b,c have almost the same intensity whereas much more AWB is visible in Fig. 2c than in Fig. 2b. The barotropic governor cannot thus explain, in this particular case, the large difference of wave breaking. Other processes should be involved such as those described in the rest of the paper.

a. Single storms effect

The aim of this section is to illustrate with examples the role of wave breaking in the NAO as well as to emphasize the effect of single storms, in particular those developing on the east coast of the United States.
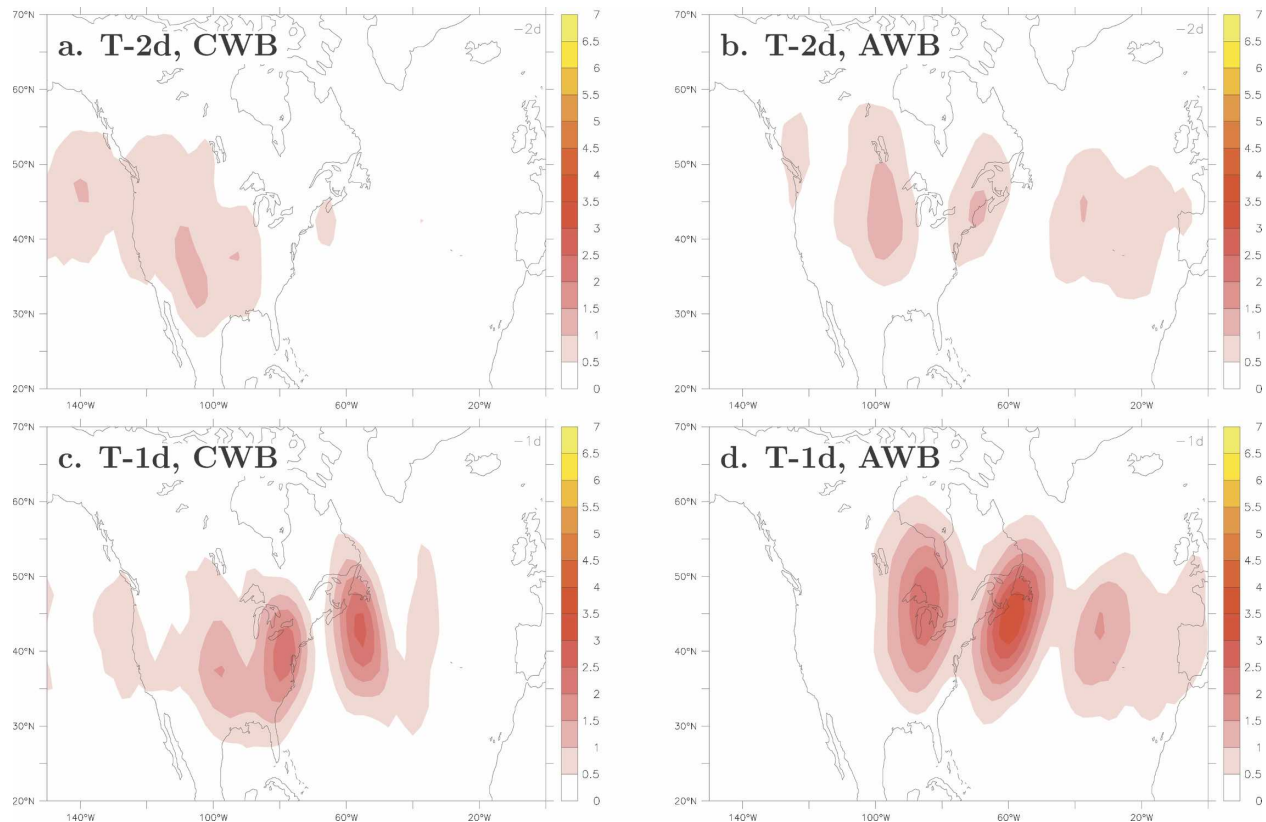
FIG. 7. Time-lag regressions of the high-frequency meridional wind amplitude (m s^{-1}) at 300 hPa based on two indexes. The left column index is based on the time series of the fluxes at 300 hPa averaged over the area 40°–50°N, 50°–40°W for days when this average is positive. The right column index is based on minus the fluxes averaged over the same area when this average is negative (see appendix B for more details). The period considered corresponds to the winter months (DJF) from 1950 to 1999.

February 1978 was a strongly negative NAO month and the time variation of the normalized daily NAO index during this month is displayed in Fig. 3a. It decreases rapidly during the first ten days until reaching a value close to −3 and then slowly increases but stays negative during the entire month. In fact, a strong snow storm hit the east coast of the United States between 5 and 7 February (see Kocin and Uccellini 1990) at the same time that the NAO index began to rapidly decrease. The latitudinal position of the low-frequency zonal wind averaged between 60° and 0°W (Fig. 3c) exhibits a rapid southward displacement of the jet, which logically corresponds to the rapid decrease of the NAO index in the beginning of the month. The end of the life cycle of the storm was characterized by CWB. This can be seen from the strongly negative momentum fluxes around 7 February (see Figs. 3c,e) as well as from the total geopotential field in Fig. 3e where wave breaking is well visible in the northeast coast of the United States. It suggests that this wave breaking is in a large part responsible for the rapid southward shift of the Atlantic jet and therefore for the rapid decrease of the

NAO index in the beginning of the month. The slow increase toward 0 after 10 February seems to be linked with another phenomenon that has longer time scales. This can be done by different processes; temperature anomalies can be dissipated by local mixing as proposed by B04 and/or by the restitution of the climatological subtropical jet position controlled by the meridional circulation of the local Hadley cell. It seems that either mechanism could create this process of weekly time scales rather than daily.

Let us now analyze a positive NAO month, March 1993. The daily NAO index (Fig. 3b) during this month has a strong increase in the middle of the month between 12 and 17 March, and is coherent with the sudden poleward shift made by the low-frequency jet from 30° to 55°N during this period (Fig. 3d). At the beginning of the same period, the East Coast was hit by a very strong storm (13–15 March 1993) with unusual intensity that led to heavy snowfall. Kocin et al. (1995) called it a superstorm, and its mechanism was analyzed by Orlanski and Sheldon (1995). The momentum fluxes over the Atlantic associated with the end of life cycle of this
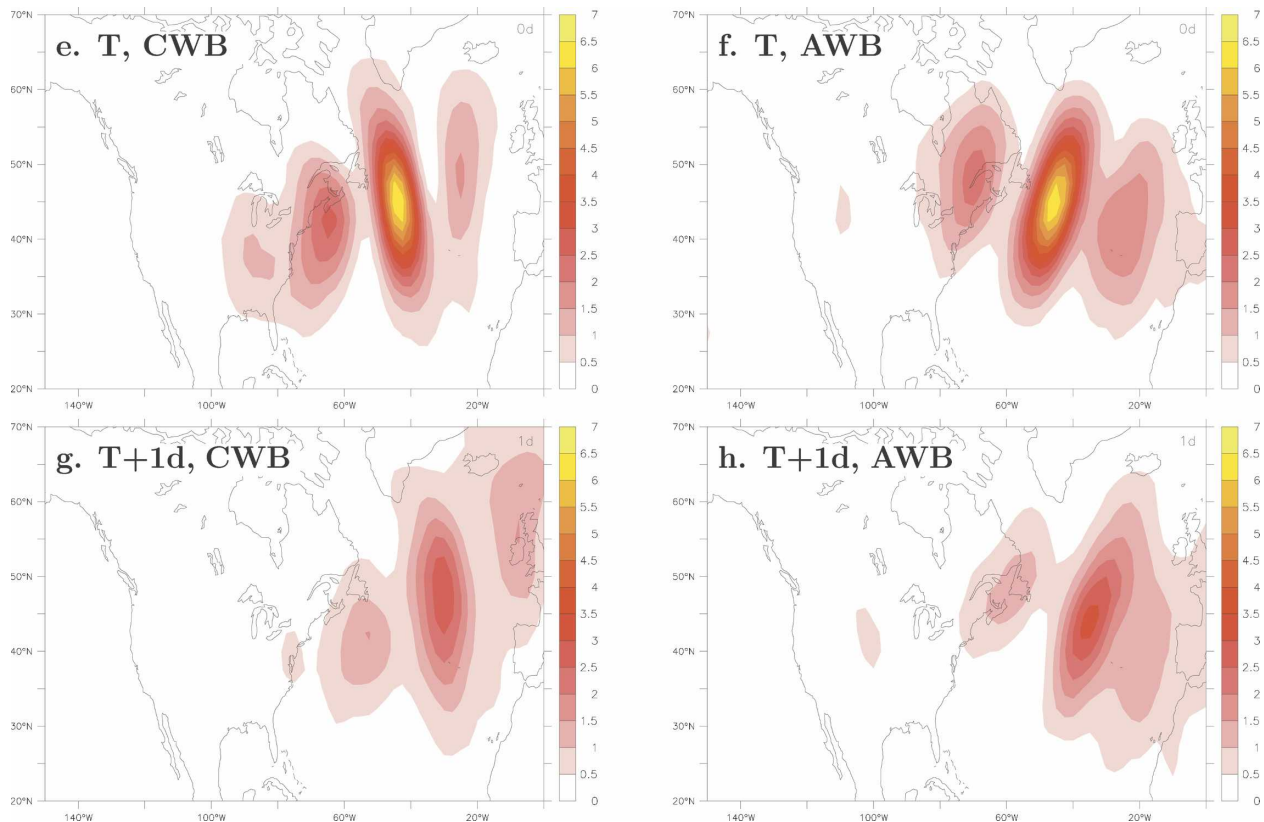
FIG. 7. (*Continued*)

storm are strongly positive around 16 March (Fig. 3d). The two-dimensional plots of Fig. 3f show that these positive fluxes are directly related to the shape of the geopotential isolines that present a clear anticyclonic wave breaking signal over the Atlantic. Note that here again we check the close relationship between the sign of the momentum fluxes and the type of wave breaking. This strong anticyclonic wave breaking offers an explanation for the rapid poleward shift of the jet at that time and the abrupt increase of the NAO index.

These results suggest that single extratropical storms can be responsible for the sign of the NAO during a quite long period, even a month. Indeed, high-frequency eddies can change the mean circulation significantly in only few days while the processes leading to the return to equilibrium requires generally weekly time scales.

b. Time lag between wave breaking and NAO events

A similar result as that shown with single storms can be found from a statistical point of view is displayed in Fig. 4. The plots represent time-lag regressions based on the momentum fluxes averaged over the Atlantic.

The regressed variables are the NAO index (black curve) and the high-frequency momentum fluxes averaged over the Atlantic (red curve). The regressed momentum fluxes are logically maximum at lag 0 days by construction of the regression. This maximum is associated with a strong increase of the NAO index at that time and a peak of the NAO index regression occurs 2 days later. It proves that wave breaking tends to occur prior to an NAO event and that it triggers its growth. The decrease of the NAO index from lag +2 is slower than the preceding increase triggered by synoptic eddies. This slower process could be due to mixing or to the return to equilibrium of the Hadley cell circulation as previously discussed.

c. Representation of wave breaking in the model

High-frequency momentum fluxes during the two consecutive months of D87 and J88 are presented in Fig. 5 as well as those for the control and modified runs discussed in section 3. Since the 31-point filter needs 31 consecutive days to compute the high-frequency signal at a given time, it cannot be used to study our simulations that are run for only 30 days. In this section, we replace this filter by another one with a less sharp cutoff
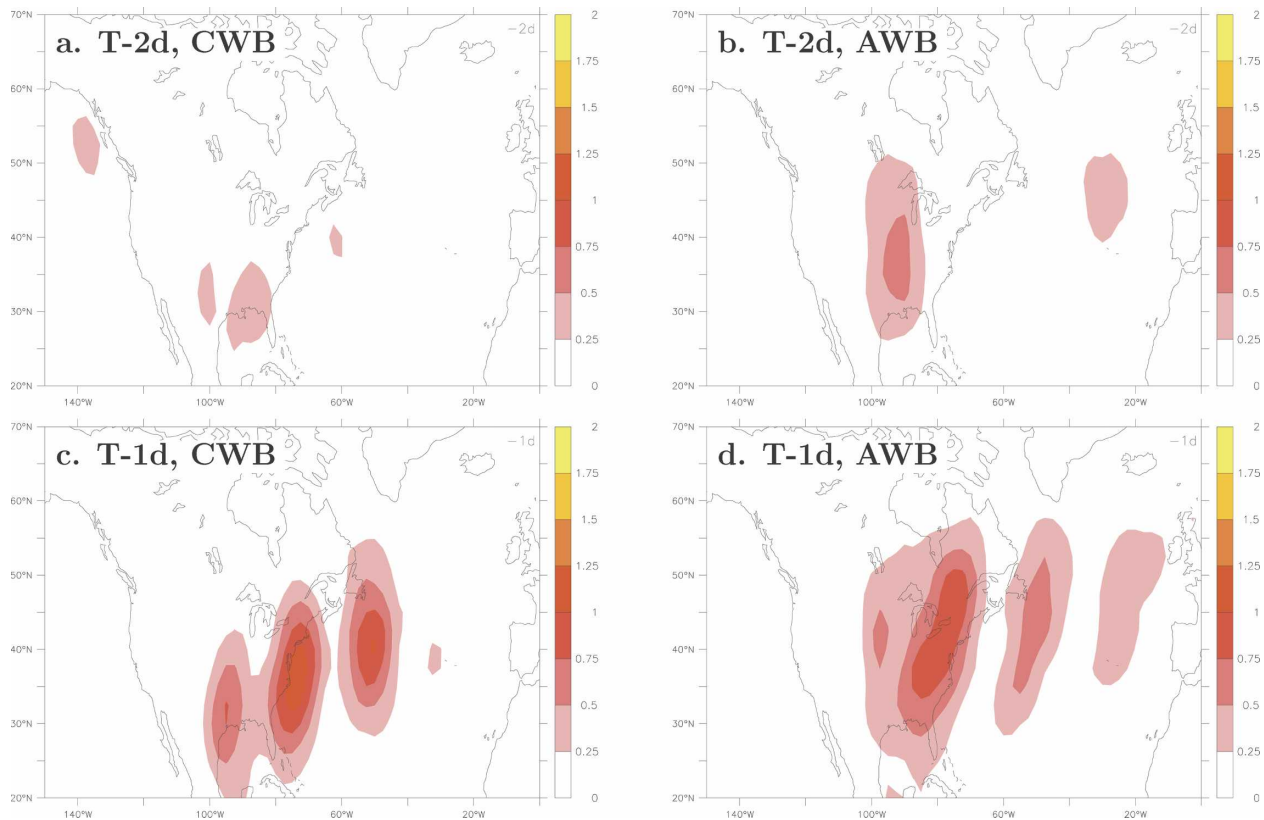
FIG. 8. Regressions with the same index as in Fig. 7 but the variable is now the high-frequency meridional wind amplitude (m s^{-1}) computed in the low levels at 850 hPa.

but which needs only an interval of 8 days to be computed (see appendix A for a more detailed description). By using an extension with reanalysis data before the initial time of the runs (1 December), the filter allows us to estimate the high-frequency flow in our simulations from day 1 to day 26.

Momentum fluxes averaged during D87 are shown in Fig. 5a and exhibit strong anticyclonic wave breaking over the eastern Pacific and North America while over the Atlantic domain, momentum fluxes have a much weaker amplitude and both signs of wave breaking appear. The strong AWB signal in the eastern Pacific suggests that waves have lost a lot of energy upstream before entering the Atlantic domain. By contrast, during J88 (Fig. 5b), strong anticyclonic wave breaking occurs over the Atlantic domain and almost no signal is present upstream of it. This wave breaking difference in the Atlantic can explain the fact that D87 and J88 were negative and positive NAO months, respectively.

High-frequency momentum fluxes for the control run displayed in Fig. 5c are strongly positive over North America whereas both negative and positive fluxes are of equal importance over the Atlantic, which is similar to what happened during the D87 month (Fig. 5a). By

contrast, the signal of the fluxes for the modified run (Fig. 5d) is very close to that of the real J88 month (Fig. 5b) with strong anticyclonic wave breaking in the Atlantic. The time–latitude plot of Fig. 5f (modified run) exhibits three significant AWB events over the Atlantic. The second one occurs in the middle of the run exactly at the same time as the Atlantic jet moves rapidly poleward, which strongly suggests that the AWB event is responsible for the jet displacement. This interpretation of the Atlantic jet transition in terms of synoptic eddy activity is confirmed by the fact that no low-frequency wave coming from the Pacific was detected during this period (not shown). Furthermore, the time–latitude plot for the control run (Fig. 5e) confirms the important role played by synoptic eddies. The jet stays at the same latitude during the first half of the control run when no sign of synoptic activity is visible over the Atlantic. By contrast, a slow poleward move of the jet starts during the second half of the control run when some synoptic activity and AWB events appear.

The model is thus able to reproduce the eastward propagation of the waves as well as their breaking inside the whole domain by only prescribing the spatiotemporal form of the flow at the western boundary
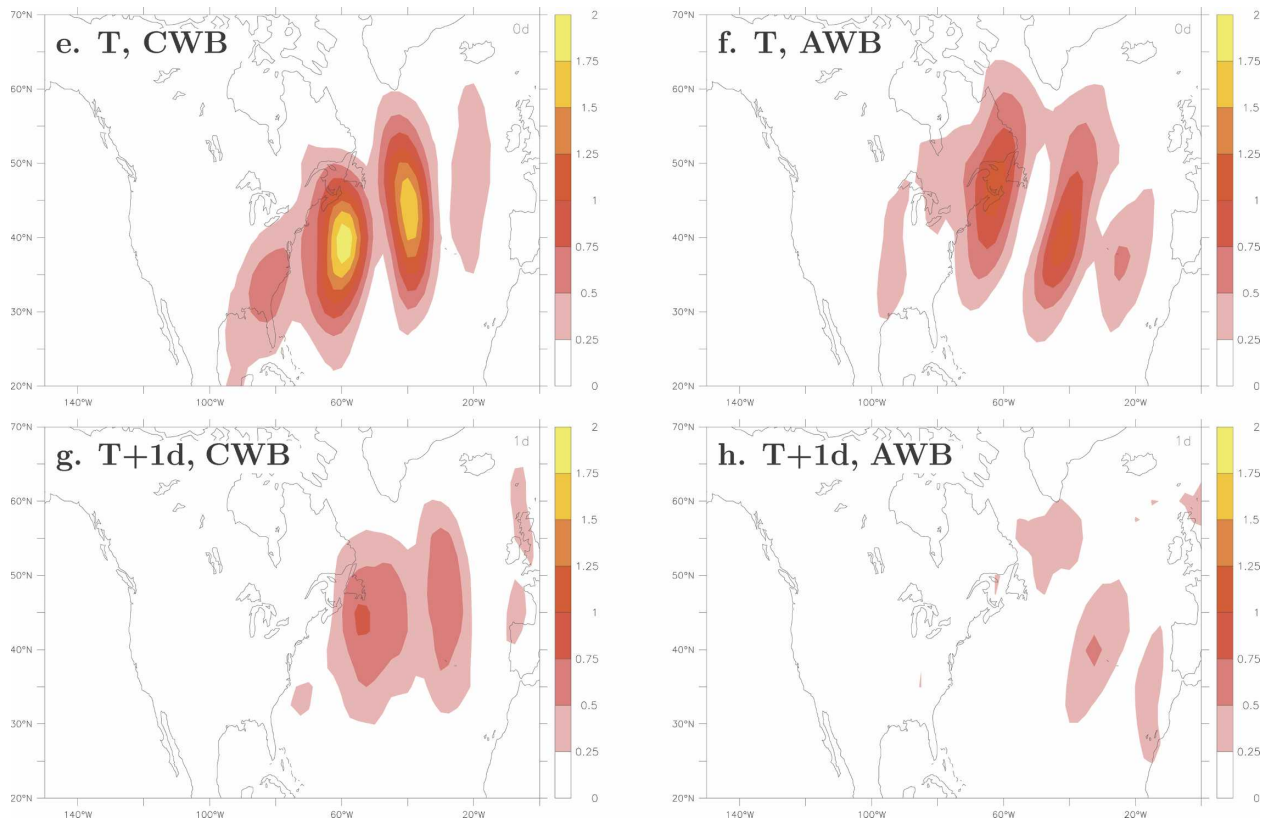
FIG. 8. (*Continued*)

(i.e., the eastern Pacific), which is therefore of fundamental importance for the NAO. By contrast with the work of F04, the ingredient that makes the waves break one way or another is not related to the initial latitude of the perturbations in the Pacific; during the two different months studied, eddy kinetic energy was located almost at the same latitude. Rather, the difference seems to come from the energy and frequencies of the waves. For D87, eddies in the Pacific have strong energy and lower frequencies that make them break strongly anticyclonically over North America; this leads to a large loss of energy at that place and eddies have therefore insufficient energy when they reach the Atlantic domain. By contrast, for J88, eddies in the Pacific are not so strong; they grow as they propagate eastward and break strongly anticyclonically over the Atlantic domain, pushing the jet more poleward in this region and creating a more positive NAO. To summarize, strong wave breaking on western North America prevents upper-level waves continuing their eastward propagation toward the Atlantic and creates a lack of waves in the latter region. As upper-level waves tend generally to break anticyclonically, a deficiency of such waves will avoid the formation of a positive phase of

the NAO and is rather characteristic of the negative phase. Note that the exact role played by the low-frequency Pacific flow in producing these different synoptic eddy activities cannot be determined from our experiments as the total flow has been implemented at the western boundary. A more systematic study on this aspect will be the aim of a future work.

5. Cyclonic and anticyclonic wave breaking processes

In this section, we analyze the difference between CWB and AWB processes and try to reach an understanding of what makes the waves break one way or another. Our approach consists in looking at the two different processes in a small area in the western North Atlantic (40°–50°N, 50°–40°W). This region, hereafter called area A, has been chosen in particular because the regressed momentum fluxes on the NAO index (Fig. 2a) present a peak in this region. Moreover, the regressed geopotential field on the time series of the averaged momentum fluxes over area A, presents a clear dipole anomaly pattern over the Atlantic, which is characteristic of the NAO (Fig. 6). Wave breaking in this
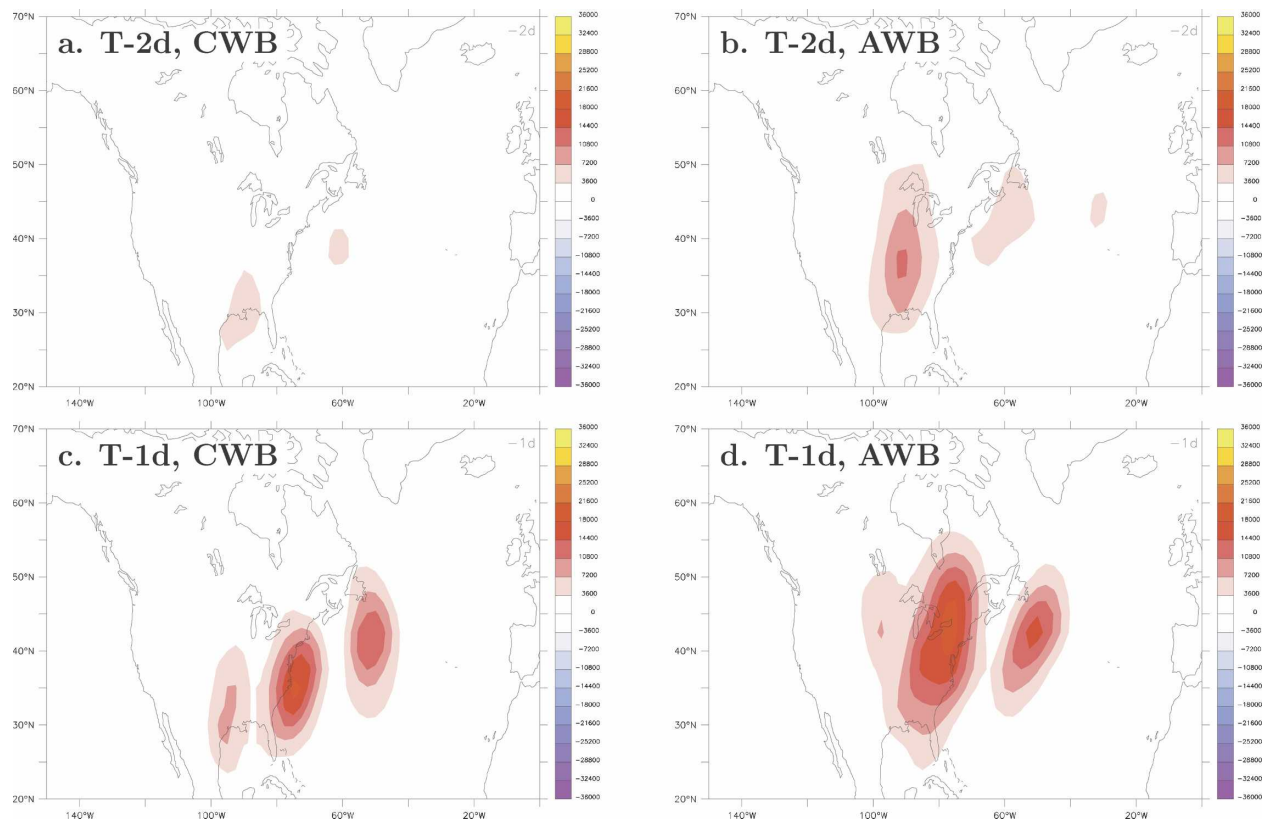
FIG. 9. Same regressions as in FIG. 7 but the variable is the meridional moist static energy fluxes per unit mass (contour interval is 3600 m³ s⁻³) computed in the low levels at 850 hPa, which is the sum of the sensible and latent heat fluxes as the geopotential fluxes are negligible.

region is thus particularly important for the NAO. Although a regression takes into account both signs of the momentum fluxes; that is, CWB and AWB processes, it does not allow a comparison of the two processes. To avoid this problem, we split the signal into two parts as follows. On the one hand, AWB can be represented by a regression where the index is the averaged momentum fluxes over area A by considering only the days when this average is positive. On the other hand, CWB is defined as the regression where the index is equal to minus the averaged fluxes in the same area A and by taking into account only the days where this average is negative (more details about this decomposition is given in appendix B). These two regressions correspond to the two types of wave breaking that occur in the upper levels in a specific region at the entrance of the Atlantic storm track and will be shown to be useful to underline the differences between the two processes. We have checked that an approach using anomaly composites that pick up only the extreme negative and positive values of the momentum fluxes in the area A lead to the same results as the two regressions previously described.

Note also that for these two particular regressions, a 12-day high-pass filter is directly applied to the twice-daily dataset and not to the daily average dataset. Since the indexes of the two regressions are based on a specific area, A, lags in time and space play an important role and a daily average would tend to smooth the signal too strongly.

a. Surface development and meridional fluxes

Figure 7 compares the two regressions in terms of wave amplitude in the upper levels at different time lags. Consistent with the definition of the two regressions, at lag 0 day, the typical tilts associated with CWB and AWB phenomena appear in Figs. 7e,f over the area A. Let us investigate what happens in the lower levels when the two types of wave breaking occur in the upper levels. Figure 8 presents two regressions based on the same indexes but the regressed variable is now the high-frequency meridional wind amplitude in the low levels (850 hPa). Major differences are visible between the two processes. First, at lag 0 day, the amplitude for the CWB case (Fig. 8e) is twice the amplitude of that for the AWB one (Fig. 8f) whereas at the same lag but
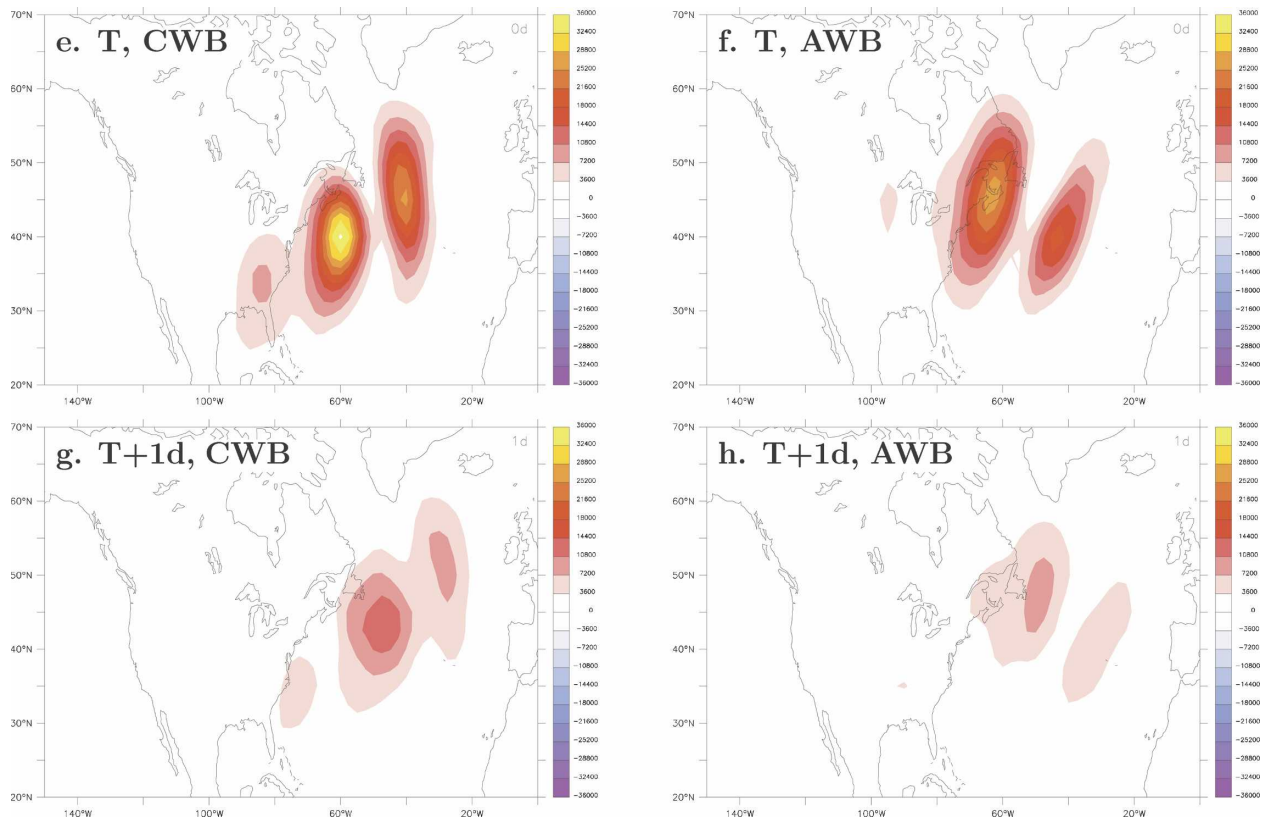
FIG. 9. (*Continued*)

in the upper levels (Figs. 7e,f) the waves have the same amplitude. It means that when CWB in the upper level occurs, it is significantly correlated with a wave development at the surface whereas the correlation is much weaker in the AWB case. Another remarkable difference can be seen from the growth rates. At lag −2 days, the wave that will break anticyclonically 2 days later (Fig. 8b) is already well visible and its amplitude is stronger than the wave that will break cyclonically at the same time lag (Fig. 8a). The growth rate between −2 days and 0 day is therefore much stronger for CWB than for AWB. This explosive surface wave growth characterizing CWB is consistent with the results of Or03 who shows that a stronger baroclinicity will tend to destabilize the low levels and lead more to CWB than AWB.

Figure 9 presents the two same regressions for the meridional moist static energy fluxes in the low levels (850 hPa). The fluxes are collocated with the wave amplitude shown in Fig. 8. Note first the difference at lag 0 day; in the CWB case (left column) the fluxes are stronger than in the AWB case (right column). The moist static energy fluxes here are approximately the sum of the sensible and latent heat fluxes. One can show that the difference between CWB and AWB fluxes do not come from the sensitive heat fluxes but is entirely due to the difference in the latent heat fluxes that are displayed in Fig. 10. The amplitude of the latent heat fluxes regression for the CWB case (Fig. 10a) is indeed twice that for the AWB case. The explosive growth rate seen at the surface in Fig. 8 in the CWB case can thus be explained by strong moisture fluxes.

At lag −2 and −1 days in Fig. 9, we see that the moist static energy fluxes are coming from the Caribbean region. This remark has to be linked with the anomaly composite of precipitable water for negative NAO displayed in Fig. 11a and leads to the following mechanism. During negative NAO, more humidity than usual is present in this region located slightly upstream of the Atlantic domain. The circulation will be thus more able to pick up this humidity and to develop large moisture fluxes that will produce a rapid destabilization of the low levels and therefore creates more CWB than AWB. This will push the jet southward and promote more the negative phase of the NAO. This possible mechanism could be particularly relevant to study the link between the NAO and other phenomenon of the climate system. The Caribbean region being in the subtropics at the
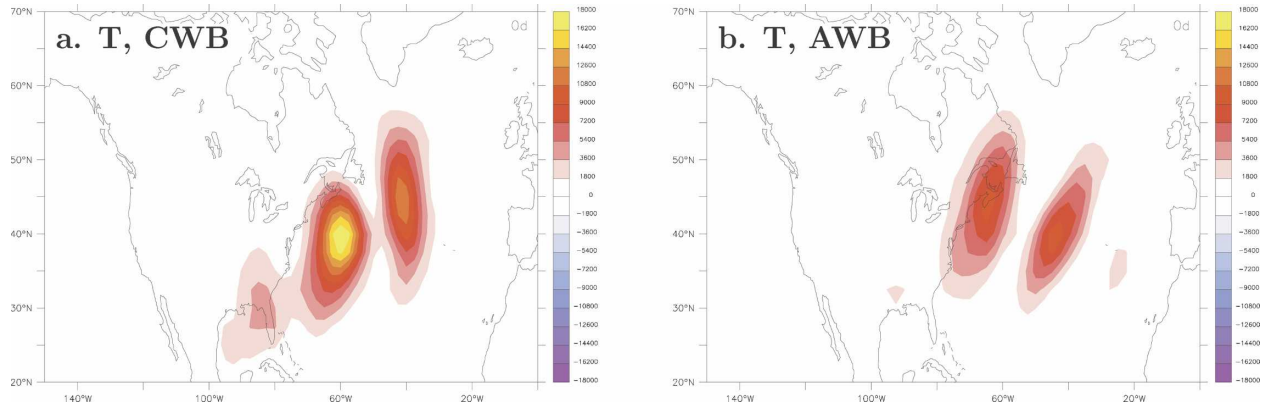
FIG. 10. Same regression as in Figs. 9e,f (i.e., with 0 time lag) but the variable is the high-frequency meridional latent heat fluxes per unit mass $L_v v'q'$ (contour interval is 1800 m^3 s^{-3}) at 850 hPa.

boundary between the Pacific and the Atlantic, anomalies in the Pacific could directly influence the weather in this region and then influence the NAO. An example of such possible links is given in section 7.

Or03 describes the difference between CWB and AWB in terms of vortex interactions (see his section 4d) and the exposed mechanism can be summarized as follows. When anticyclones are stronger than cyclones, the latter are stretched along the SW–NE direction by the circulation formed by the anticyclones that are east and west of them. This configuration leads to AWB. By contrast, when anticyclones become less intense than cyclones, the latter are responsible for the elongation of the former along the NW–SE direction and CWB becomes predominant. The high-frequency relative vorticity regression maps shown in Figs. 12a,b support this explanation. The AWB regression (Fig. 12b) is indeed characterized by an elongated cyclone located between two anticyclones whereas the CWB regression (Fig.

12a) is formed by an anticyclone surrounded by two cyclones consistently with the schematic picture of Fig. 9 of Or03. This vortex interaction mechanism lead to a rationale for the surface effects discussed previously. Strong surface moisture fluxes will help to destabilize the low levels and will result in an important cyclonic development. In this case, cyclones are more intense than anticyclones and CWB will predominate. While different studies (e.g., T93; Lee and Feldstein 1996) have emphasized the role played by the shearing components of the basic state and the refractive index in the control of wave breaking, our results indicate that the relative strength between cyclones and anticyclones can be also an important factor to determine the type of wave breaking.

b. Difference in frequencies

Some panels of Fig. 7 suggest that waves breaking anticyclonically have a larger spatial scale than those
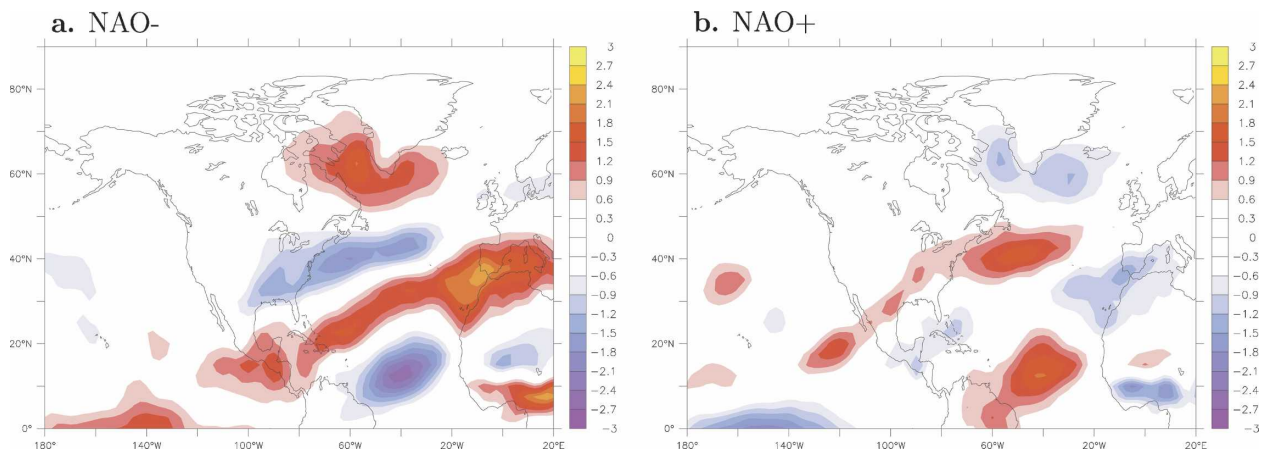

FIG. 11. (a), (b) Anomaly composites of precipitable water (kg m^{-2}) for values of the NAO index above 1 and below −1 (1 being the standard deviation) for winter months (DJF) from 1950 to 1999. Data used are monthly values.
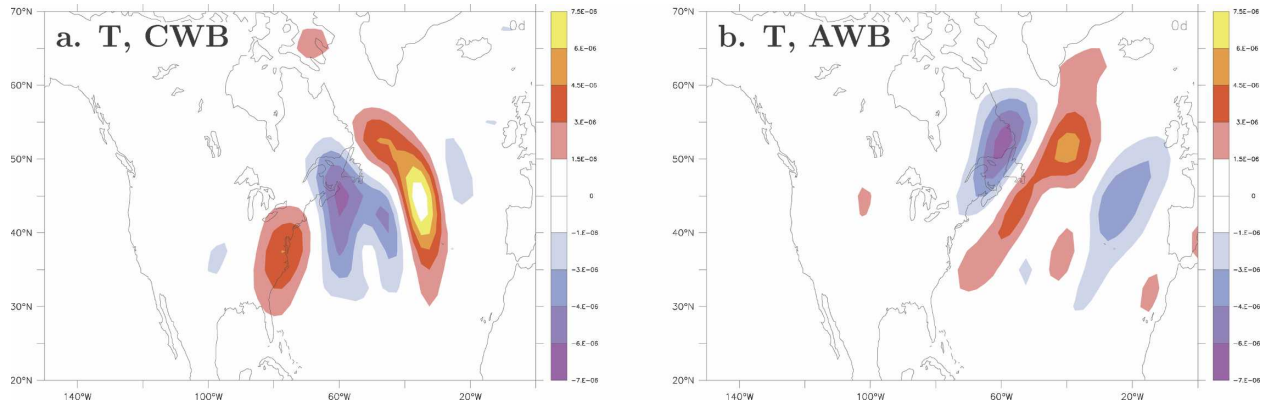
FIG. 12. Same regression as in Figs. 7e,f (i.e., with 0 time lag) but the variable is the high-frequency relative vorticity (s^{-1}) at 300 hPa.

breaking cyclonically (e.g., cf. Figs. 7c and 7d) and the aim of the present section is to investigate this aspect. The results of Or03 have already shown a strong sensitivity to the wavelength of the waves and Fig. 13 of the present paper, directly derived from Fig. 18a of Or03, summarizes these effects. The figure exhibits a transition curve diagnosed numerically in a shallow water model between poleward and equatorward shifts of the zonal jet in a two dimensional space formed by, on the one hand, the amount of eddy kinetic energy and, on the other hand, the zonal wavenumber. Figure 13 further shows that for a typical range of eddy kinetic energy, waves break only anticyclonically for low wavenumbers while both CWB and AWB can occur for large wavenumbers with a predominance for CWB. This result can be understood qualitatively as follows. The shorter the spatial scale of the wave is, more important are the ageostrophic effects and, in this case, cyclones become more intense than anticyclones which promotes more cyclonic wave breaking. For large spatial scales, this strong asymmetry between cyclones and anticyclones does not exist anymore but waves tend generally to propagate equatorward due to effective beta asymmetries and to reach a critical latitude making them break anticyclonically. More details on the spatial-scale effect can be found in section 4b of Or03.

Our focus now shifts to investigate more carefully the difference between AWB and CWB in the observations in terms of the spatial and temporal characteristics of the waves and to check the validity of the theoretical curve shown in Fig. 13.

By using the 12- and 5-day high-frequency filters described in appendix A, one is able to extract from the daily average dataset the intermediate-frequency signal whose periods are between 5 and 12 days and the very-high-frequency signal whose periods are between 2 and

5 days. These bandpass and very-high-pass frequency filters are applied to the zonal and meridional wind components. Momentum fluxes for these two distinct frequency ranges are shown in Figs. 14a,b. Appendix C gives more details concerning this computation and compares it to another procedure starting directly from the twice-daily dataset.
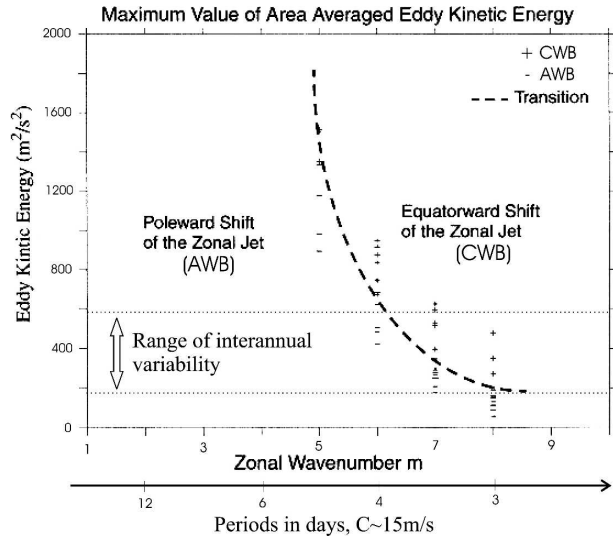
The intermediate-frequency momentum fluxes (Fig.

FIG. 13. Transition curve separating AWB and CWB processes in a two-dimensional space made by eddy kinetic energy (y axis) and zonal wavenumber (x axis) (from Orlanski 2003). By using a typical value for the phase velocity of synoptic waves in the atmosphere ($C \sim 15$ m s^{-1}), the same curve can be viewed as eddy kinetic energy (EKE) as a function of frequencies. For the energy corresponding to the range of interannual variability, intermediate waves (periods between 5 and 12 days) break anticyclonically and push the jet poleward whereas high-frequency waves (periods less than 5 days) can break both cyclonically and anticyclonically with a predominance for CWB and an equatorward shift of the jet.
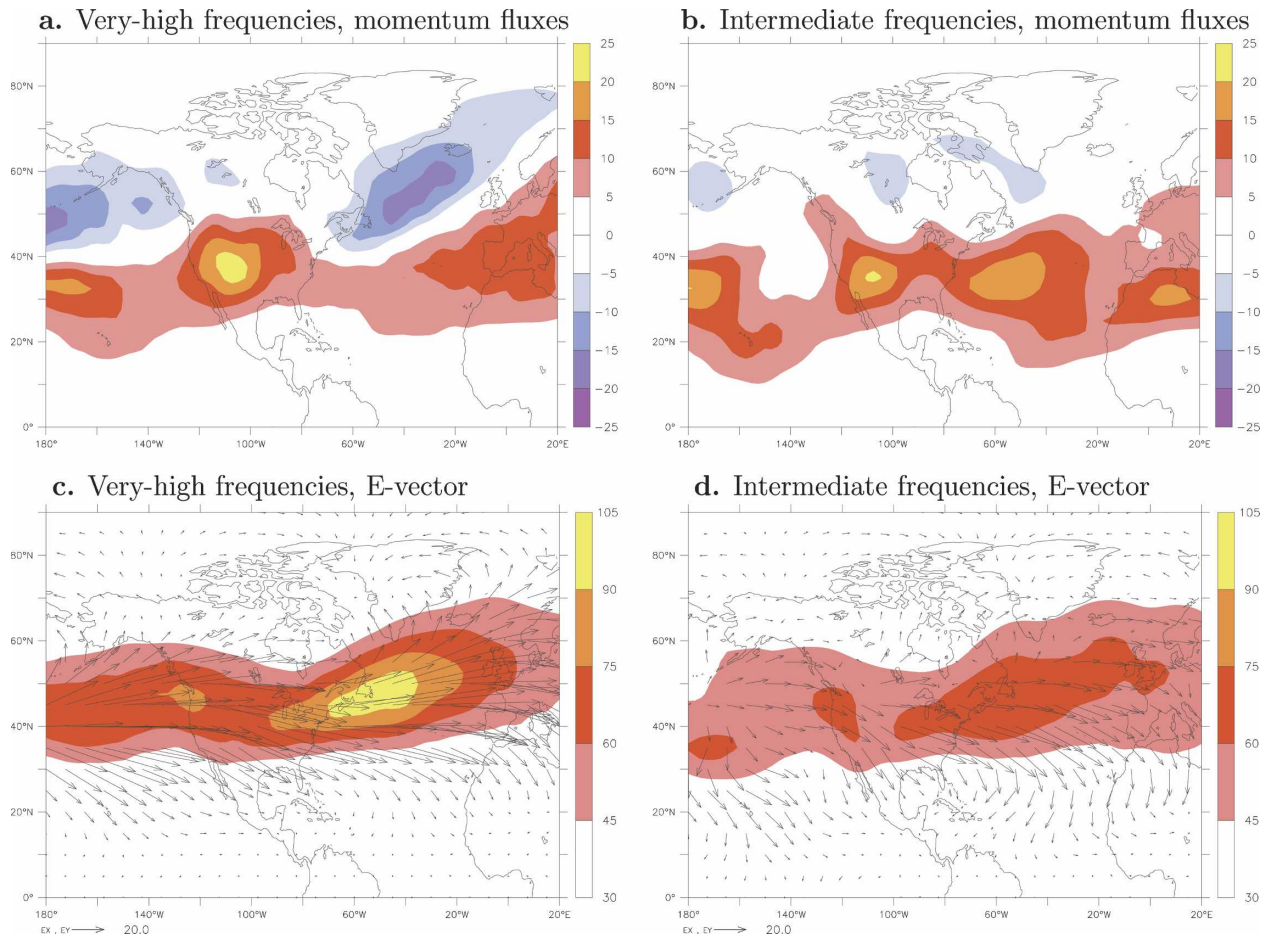
a. Very-high frequencies, momentum fluxes

b. Intermediate frequencies, momentum fluxes

c. Very-high frequencies, E-vector

d. Intermediate frequencies, E-vector

FIG. 14. The meridional momentum fluxes (color shadings, in $m^2 s^{-2}$) for (a) very-high-frequency and (b) intermediate-frequency waves. The kinetic energy per unit mass (color shadings, in $m^2 s^{-2}$) and **E** vector (arrows) for (c) very-high-frequency and (d) intermediate-frequency waves. Intermediate-frequency waves correspond to periods between 5 and 12 days and very-high-frequency waves to those less than 5 days.

14b) exhibit a strong positive signal over the Atlantic domain whereas the negative signal is almost nonexistent. By contrast, momentum fluxes for the very high frequencies (Fig. 14a) can be positive and negative with slightly stronger amplitudes on the negative side. If you consider now the range of interannual variability in Fig. 13, one can see that all the intermediate frequencies are on the left side of the transition curve and can only break anticyclonically. By contrast, the transition curve is located in the very-high-frequency domain (for the same range of variability), and both anticyclonic and cyclonic wave breaking can occur. As the sign of the momentum fluxes is a proxy to quantify wave breaking, Fig. 13 and Figs. 14a,b are therefore very consistent with each other.

Figures 14c,d complete the picture by comparing the behavior of these two different frequency ranges in terms of kinetic energy and the **E** vector. The divergence of the **E** vector is directly related to the eddy feedback as it can be seen from Eq. (3) and is a useful parameter to estimate the direction of wave propagation. Figure 14 leads to the following conclusions; waves in intermediate frequencies break essentially anticyclonically and propagate equatorward (the **E** vector points equatorward in Fig. 14d) accelerating the mean zonal wind north of their propagation. By contrast, waves in very high frequencies can break both cyclonically and anticyclonically with a slight dominance for cyclonic wave breaking and can propagate in both directions.

Note also that Fig. 14 can be viewed as a continuation of the results of Hoskins et al. (1983) who have shown that high-frequency eddies with periods less than 10 days tend preferentially to propagate equatorward (the **E** vector is predominantly equatorward especially at the end of the storm track). The result is also found for the high-frequency range defined in our paper (periods less than 12 days). However, behavioral differences in-
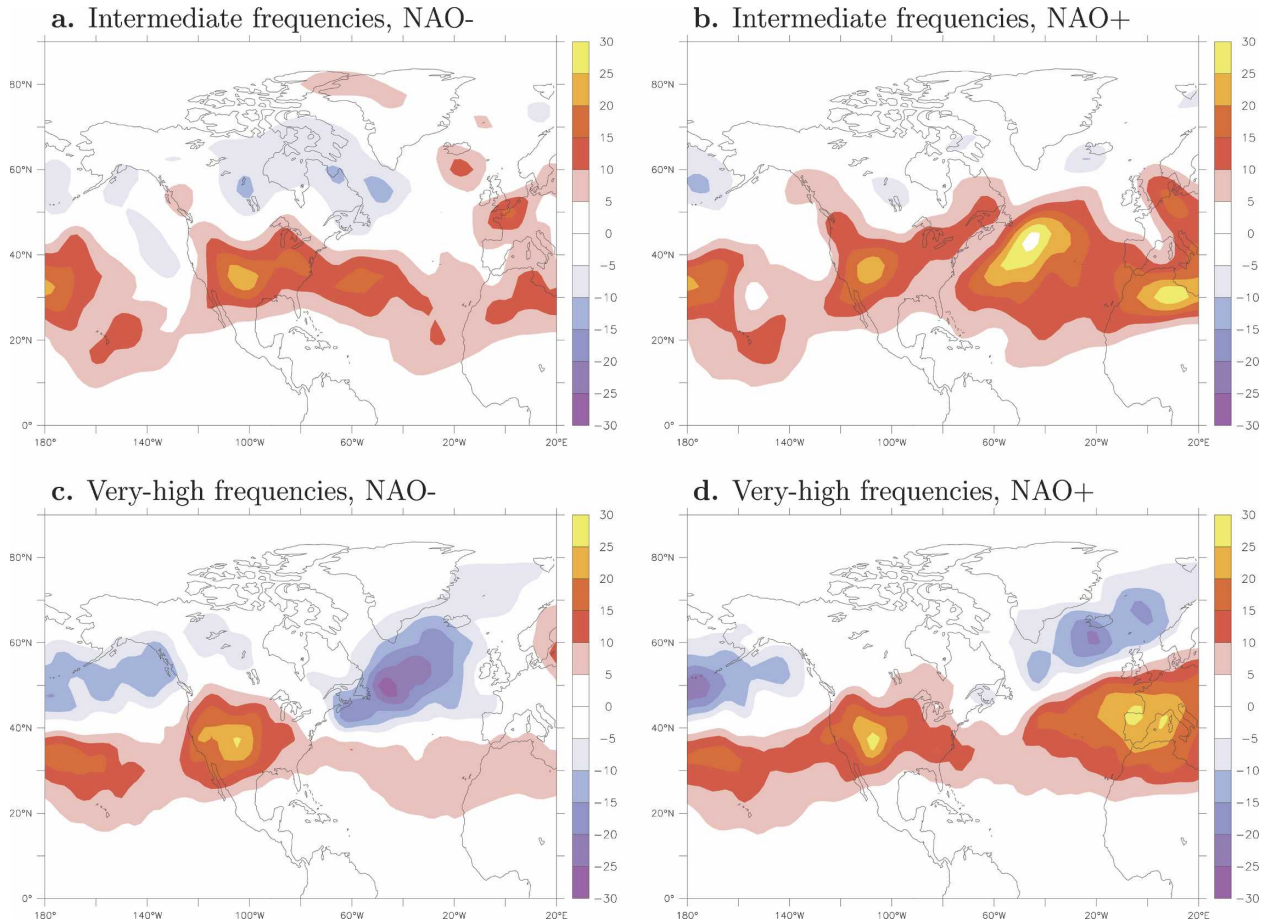
a. Intermediate frequencies, NAO-

b. Intermediate frequencies, NAO+

c. Very-high frequencies, NAO-

d. Very-high frequencies, NAO+

FIG. 15. Monthly composites for (a), (c) negative NAO (index less than −1) and (b), (d) positive NAO (index greater than 1) of momentum fluxes ($m^2 s^{-2}$). (a), (b) The momentum fluxes for intermediate-frequency waves (periods between 5 and 12 days) and (c), (d) for very-high-frequency waves (periods less than 5 days).

side the synoptic-scale frequency range were not considered in the previously mentioned paper and a new information is here given by contrasting the two columns of Fig. 14. The preference for equatorward propagation (or equivalently positive momentum fluxes) is coming from the intermediate frequency subrange and not from the very-high-frequency one.

All the panels of Fig. 14 are general in the sense that they do not involve the NAO phenomenon in any way; they are just winter averages from 1950 to 1999. Figures 15a–d complement the results of Fig. 14 by showing the momentum fluxes for intermediate and very-high frequencies for the two different phases of the NAO. Momentum fluxes for intermediate frequencies are essentially positive for both signs of the NAO, but those for positive NAO (Fig. 15b) are significantly stronger than those for negative NAO (Fig. 15a). This is due to the fact that during positive NAO, energy in intermediate frequencies is larger than during negative NAO. Very-high-frequency momentum fluxes are strongly negative

for negative NAO (Fig. 15c) over the Atlantic suggesting strong cyclonic wave breaking while the same fluxes are both positive and negative for positive NAO (Fig. 15d). This is consistent with Fig. 13 that shows that the two types of wave breaking can occur for the very high frequencies.

c. Difference in spatial scale

A similar decomposition is done in the present section but in terms of spatial scale. We use now a spatial filter (details given in appendix A) to separate the high-frequency flow into two parts, a small-scale part that takes into account all the zonal wavelengths less than 4000 km and a large-scale part obtained by the subtraction of the small-scale part from the total high-frequency flow. Our aim is to look at the impact of the spatial scale on the synoptic-scale wave breaking. Kinetic energy averages for these two spatial scale ranges and for the two phases of the NAO are shown in Fig.
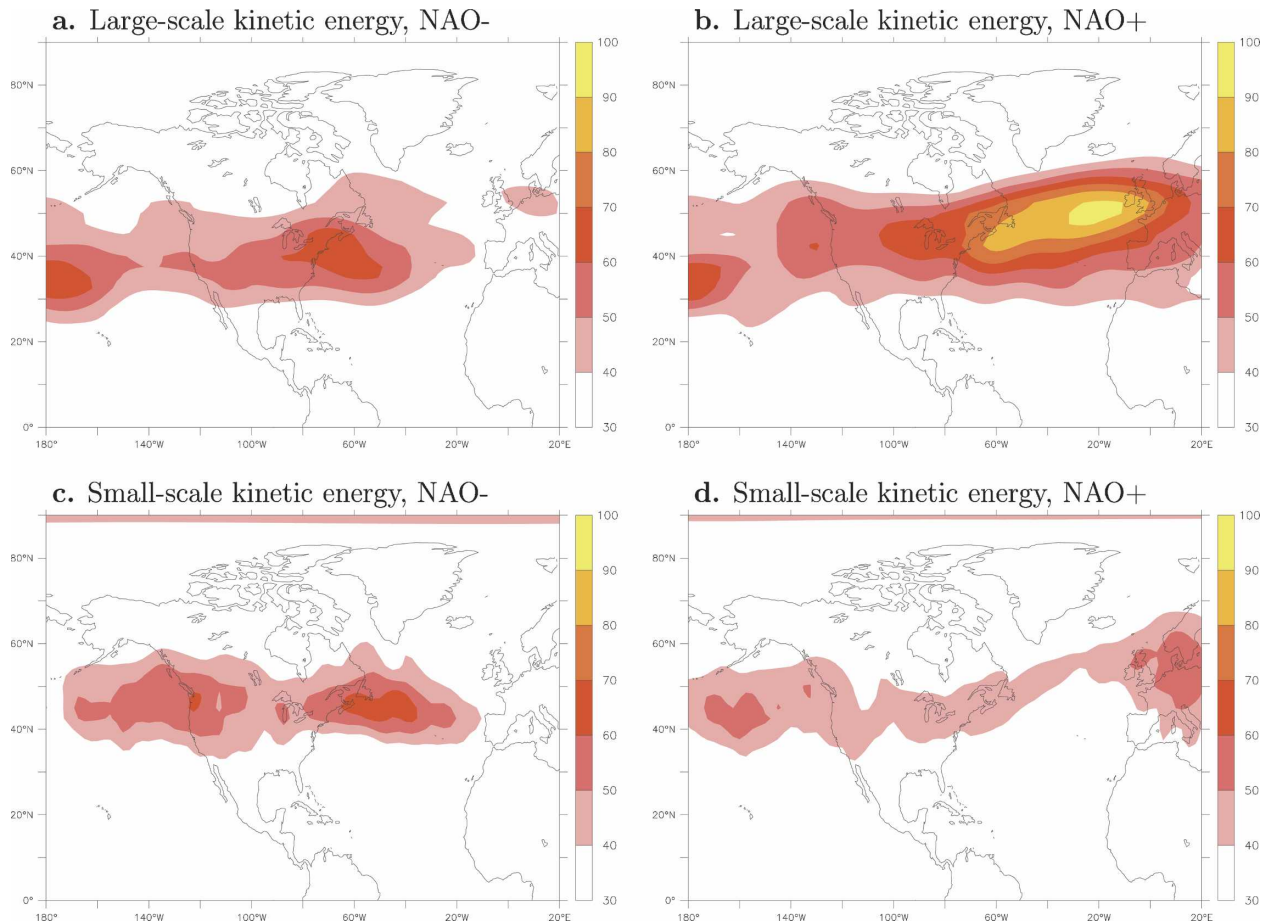
FIG. 16. Daily composites for (a), (c) negative NAO (index less than -1.5) and (b), (d) positive NAO (index greater than 1.5) of kinetic energy. The high-frequency kinetic energy per unit mass ($m^2 s^{-2}$) for (a), (b) large-scale waves and (c), (d) small-scale ones. The length-scale cutoff is around 4100 km.

16. The conclusion is that large-scale kinetic energy is stronger for the positive NAO composite than for the negative NAO one while the reverse occurs for small-scale kinetic energy.

A similar result done with the same decomposition is presented in the scatter diagram of Fig. 17. It represents small-scale kinetic energy averaged in a region centered over the Atlantic storm track versus the large-scale kinetic energy averaged in the same region. The cloud formed by the days characteristic of negative NAO (blue squares) is more located in the domain where the small-scale energy is stronger than the large-scale one while the reverse happens for the cloud formed by the positive NAO events (red circles). Waves with larger (smaller) spatial scales tend to break anticyclonically (cyclonically) and to promote more positive (negative) NAO. These conclusions on the spatial scale effect are consistent with those found in terms of frequencies and support the theoretical results of Fig. 13.

6. NAO and wave breaking on interannual and interdecadal time scales

The relations between the NAO and other phenomena of the climate system are not the principal focus of our study as our aim is more to analyze the intrinsic mechanism of the NAO, particularly with regard to the role of the Atlantic storm-track eddy activity. However, this section presents arguments for understanding how the NAO responds to external forcing or to interpret the influence of other teleconnections on the NAO. Figure 18 is a regression on the ENSO index where the variable is precipitable water. An impact of ENSO is visible in the Caribbean region where more (less) precipitable water is present during El Niño (La Niña). More humidity in this region during strong El Niño will help to destabilize the atmosphere and will create more cyclonic development in the low levels. Cyclones will become more intense; CWB is more likely to occur and
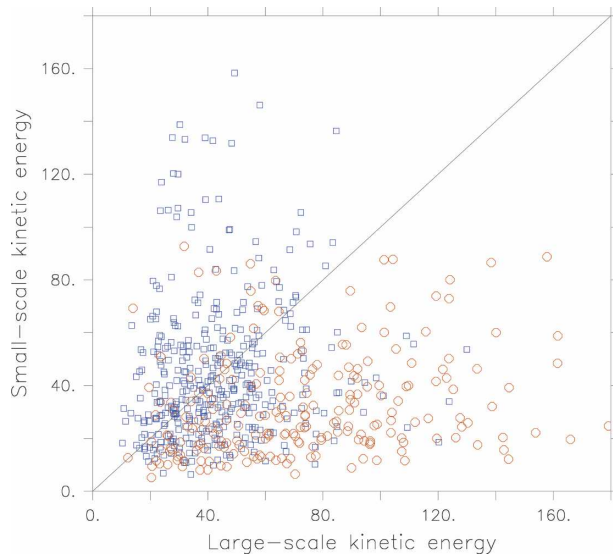
FIG. 17. Large-scale kinetic energy vs small-scale kinetic energy ($m^2\,s^{-2}$) over the Atlantic domain (35°–55°N, 60°–0°W) for daily NAO index less than -1.5 (blue squares) and greater than 1.5 (red circles).

FIG. 18. Regression on monthly Niño-3.4 (5°N–5°S, 170°–120°W) index of precipitable water (kg m^{-2}) for winter months (DJF) from 1950 to 1999.

therefore a more negative NAO results. In fact, the correlation between the NAO and ENSO is slightly negative (around -0.15) in the second half of the twentieth century and among the eight strongest El Niño during the same period, five correspond to negative NAO, two to positive NAO, and one does not have a well-defined NAO phase. We speculate that such a slight anticorrelation between the two phenomena can be explained by the mechanism previously described. It should be pointed out that, on the one hand, El Niño years bring more moisture over the western Atlantic, which promote more the negative phase of the NAO but on the other hand more upper-level waves from the eastern Pacific can enter the Atlantic domain without breaking, which will be more favorable to positive NAO than negative since upper-level waves tend generally to break anticyclonically. These two opposite effects may explain the fact that the anticorrelation between the two phenomena is only weak.

Another open question concerns the decadal trend of the NAO for which no real consensus exists (Hurrell et al. 2003). High-frequency momentum flux maps in Figs. 19a,b correspond to winter averages during the periods from 1950 to 1975 and from 1976 to 1999, respectively. Figure 19c is the difference between these averages and shows that momentum fluxes were stronger during the latter period when more positive NAO months were present than during the former one, which was characterized by more negative NAO months. Furthermore, when comparing Figs. 19a and 19b, note that the dif-
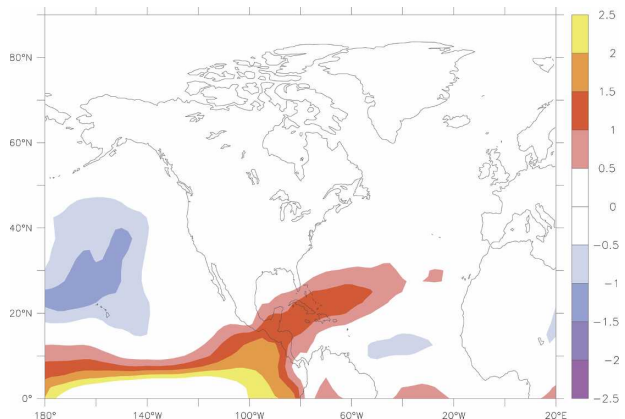
ference is essentially coming from the positive momentum flux signal whereas the negative momentum fluxes have almost the same amplitude. Anticyclonic wave breaking was therefore more present during the most recent period than during the earliest one. If one wants to explain the decadal NAO trend, it seems important to understand the external forcings outside the Atlantic domain that will make the waves break more anticyclonically during the second period in the Atlantic. For instance, some anomalies in the Pacific could affect the spatiotemporal properties of the waves that can then directly change the type of wave breaking in the Atlantic as it has been seen from our simulations. But other external factors could be important too such as the SSTs in the tropical Atlantic that can create important anomalies in the characteristics of the waves that will then promote one phase or another of the NAO. The important point we would like to emphasize is that the different mechanisms leading to AWB or CWB analyzed in the present paper may be useful to interpret the impact of external forcings on the NAO.

7. Conclusions

The crucial role played by synoptic-scale wave breaking in the NAO phenomenon was exposed in the present study. Consistent with the recent results of B04 and F04, positive and negative phases of the NAO are respectively formed by anticyclonic and cyclonic breaking of the synoptic eddies, that is, when their structures tilt respectively along the SW–NE and NW–SE direction. We have placed an emphasis on the relation between wave breaking and the classical tools to study the eddy feedback onto the general circulation such as the eddy momentum fluxes. The characteristic tilts of the
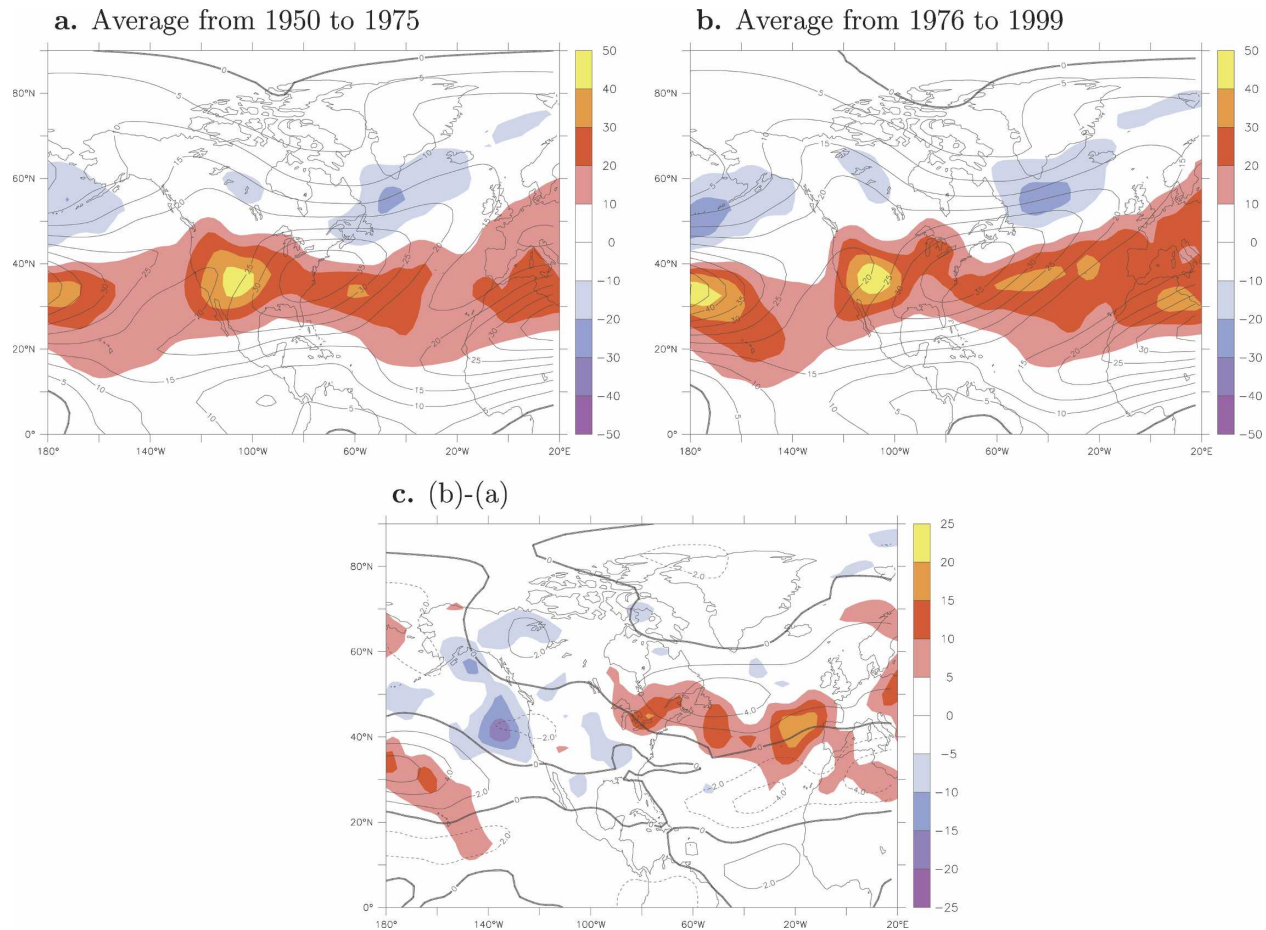
FIG. 19. (a) The time average of the zonal wind (black contours, contour interval is 5 m s^{-1}, isotachs less than 0 m s^{-1} omitted) and the high-frequency momentum fluxes (color shadings, in m^2 s^{-2}) for winter months (DJF) between 1950 and 1975. (b) Same as (a) but between 1976 and 1999. (c) The difference between (b) and (a); the solid and dashed black contours correspond to positive and negative values of the zonal wind anomalies (contour interval is 2 m s^{-1}).

two different types of wave breaking are directly related to the sign of the meridional eddy momentum fluxes. Anticyclonic and cyclonic wave breaking lead respectively to positive and negative eddy momentum fluxes. One can derive from the equation governing the low-frequency zonal wind that in the case of anticyclonic wave breaking, positive momentum fluxes push the zonal jet poleward while in the cyclonic case, negative momentum fluxes move the jet equatorward. Positive and negative NAO events that are characterized by poleward and equatorward displacement of the upper-tropospheric Atlantic jet thus logically have their origin in anticyclonic and cyclonic wave breaking respectively. It was then shown that high-frequency momentum fluxes were a useful tool to measure synoptic-scale wave breaking and that their sign was indeed directly correlated with the NAO index. During positive NAO months, positive fluxes have stronger amplitudes than

negative ones and vice versa during negative NAO months.

The important issues related to wave breaking and NAO that have been highlighted throughout the paper are the following: (i) single storm's effect, (ii) spatial and temporal characteristics of the waves, (iii) upstream influence, and (iv) surface effects.

One part of our results show that extratropical cyclones, particularly those occurring along the east coast of the United States, can have a sudden and significant effect on the Atlantic mean circulation. Such cyclones finish their life cycle over the Atlantic domain by breaking either anticyclonically or cyclonically and can quickly push the jet poleward or southward. Two examples with opposite effects have shown that even single storms can trigger important NAO events. Their breaking at the end of their life cycle can change the NAO index in few days and can affect the sign of the

NAO during an entire month as the return to equilibrium related to the Hadley cell circulation needs much longer time scales.

The rest of the paper was devoted to the factors that determine the type of wave breaking. A main conclusion is that synoptic waves with intermediate frequencies (periods between 5 and 12 days) break anticyclonically whereas synoptic waves with very high frequencies (periods between 2 and 5 days) will tend to break both cyclonically and anticyclonically with a predominance for cyclonic wave breaking. The same conclusion is valid if the separation is done in terms of spatial scale consistent with the more theoretical results of Or03; the larger (smaller) the spatial scale of the wave is the stronger the chance is for the wave to break anticyclonically (cyclonically).

Upstream influence is an important external factor determining the NAO as it has been emphasized by our simulations with the nonhydrostatic high-resolution ZETAC model. By prescribing the spatial and temporal characteristics of the flow in the eastern Pacific for the months of December 1987 and January 1988, one can derive the correct sign of the NAO index for these months, negative for the former and positive for the latter. The difference between the two months does not come from the latitudinal position of the eddies in the Pacific as in F04 but rather seems to be due to their energy and their frequencies. In the December 1987 case, waves in the Pacific have strong energy, in particular in the intermediate-frequency range and break therefore strongly anticyclonically at that place before reaching the Atlantic domain. They do not have a significant impact over the Atlantic since they already have lost their energy upstream of this domain. By contrast, in the January 1988 case, waves in the Pacific have much less energy and do not break in this region. But as they grow during their eastward propagation, their frequencies reach more and more the intermediate range. These waves break anticyclonically exactly over the Atlantic, which creates a more positive NAO type. Note that we found other months different from December 1987 but with also negative NAO signs (not shown here) that exhibit strong anticyclonic wave breaking occurring upstream of the Atlantic domain and not inside. However, it does not seem to be the general case. A more systematic analysis of upstream influence should be performed in future studies as it has direct predictability issues for the NAO and could serve to understand interactions between different regions and different teleconnections of the climate system.

While the previous factor is an external driving of the NAO, a remarkable internal feedback underlined in the paper concerns surface effects and the relation between upper and lower levels. When CWB occurs in the upper levels, it is strongly correlated with an explosive development of synoptic eddies in the low levels accompanied by strong surface moisture fluxes. AWB seems to be more characterized by upper-level waves alone with a much weaker signature at the surface. This could be explained in terms of vortex interaction as proposed by Or03. Strong surface moisture fluxes will destabilize the low levels and will promote the development of cyclones in the low levels. The cyclones become more intense than anticyclones and will stretch them along the NW–SE direction. By contrast, when such a destabilization is not present, the circulation of the anticyclones will dominate and is responsible for the elongation of the cyclones along the SW–NE direction. Note that this vortex interaction mechanism is consistent with the influence of the spatial scale on wave breaking summarized in the previous paragraph. For short waves, the ageostrophic effects in the stretching term of the vorticity equation are very important, cyclones can reach much stronger amplitudes than anticyclones that will make the waves break more cyclonically.

To conclude on the perspective of this study, some of our results suggest that answering the question why waves break cyclonically or anticyclonically cannot only improve our understanding of the NAO on short time scales but also can serve as a basis to study the variations of the NAO on longer time scales such as its interannual and interdecadal fluctuations. Of course, other processes can influence the variations of the NAO or AO without necessarily involving wave breaking such as the downward propagation of stratospheric anomalies but synoptic wave propagation and its breaking is a potential candidate to explain the link between different teleconnections of the climate system.

APPENDIX A

Spatial and Temporal Filters

Most of the figures involve the 31-point Lanczos high-pass filter with a 12-day cutoff that separates the

a. 31-point filters for daily dataset   **b.** 17-point filter for twice-daily dataset
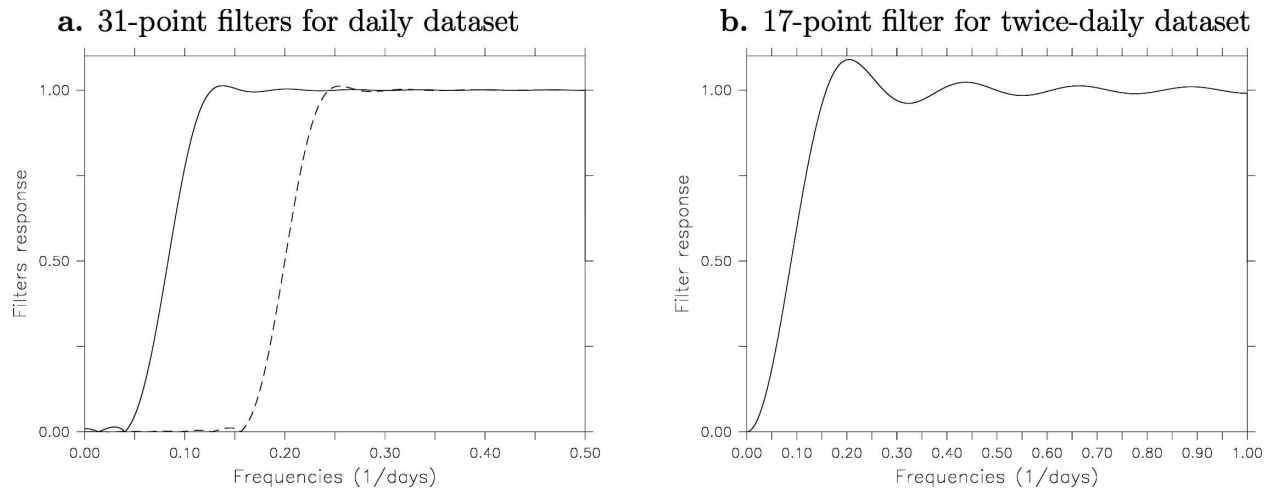

FIG. A1. (a) Response function of the two 31-point Lanczos high-frequency filters applied to a daily dataset. The solid and dashed lines correspond to the filters with cutoff at a period of 12 and 5 days, respectively. (b) Response function of a 17-point high-frequency filter applied to a twice-daily dataset. Its cutoff is around 12 days and is used to get Fig. 5. The filter is less sharp and less accurate than the ones shown in (a) but allows one to estimate the high-frequency flow in our 30-day runs.

synoptic high-frequency signal from the rest of the flow [see Duchon (1979) for a description of the Lanczos filters]. Its response function is displayed in Fig. A1a as well as that of the 31-point Lanczos high-pass filter with a 5-day cutoff. This second filter was also used to define the intermediate (periods between 5 and 12 days) and very-high frequency (periods between 2 and 5 days) ranges.

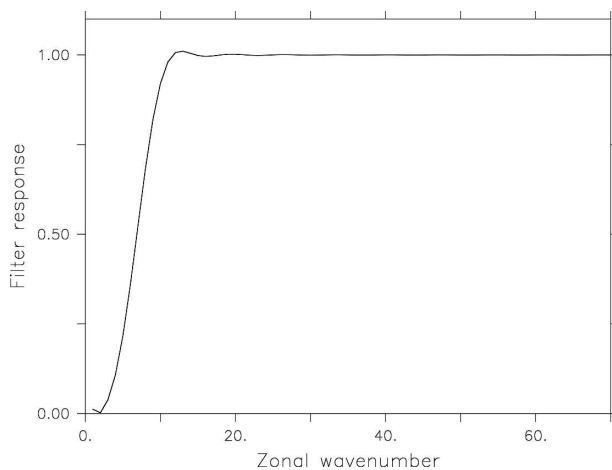The 31-point filters are applied to a daily dataset and

FIG. A2. Response function of the low-pass zonal wavelength Lanczos filter with a cutoff of 4100 km. This filter was used to get Figs. 16 and 17. At 45°N, the cutoff corresponds to wavenumber 7 as it can be seen from the figure. However, in order to filter the signal at a given length scale (4100 km) and not at a given wavenumber 7, the cutoff coefficient applied in the Lanczos filter at other latitudes depends on the cosine of the latitude. See appendix A for more details.

need therefore 31 consecutive days to get the high-frequency signal at a given time. To estimate the high-frequency signal in our simulations that are run only during 30 days, we apply another filter with a less sharp cutoff but has the advantage to be computed with only eight consecutive days. More precisely, this is a 17-point filter applied to a twice-daily dataset with a cutoff around 12 days and its response function is shown in Fig. A1b. This filter therefore allows the computation of the high-frequency flow within an interval between +4 days and +26 days after the initial time of each simulation. Furthermore, as the two simulations are started with the reanalysis dataset of 1 December, we have extended the data of the control and modified runs with the reanalysis dataset at the end of November 1987 in order to get also an estimate of the high-frequency flow between 0 days and +4 days. Figures 5c,d correspond to averages of the high-frequency flow for the two runs between +0 day and +26 days after the initial time of the simulations.

In Figs. 16 and 17, a low-pass zonal wavelength filter with a cutoff around 4100 km was used to decompose the high-frequency flow into two different parts, a large-scale high-frequency flow and a small-scale high-frequency flow. Since our data is on a 2.5 grid, we dispose of 144 grid points at a given latitude. At 45°N, the cutoff applied in the Lanczos filter corresponds to 21 grid points (around wavenumber 7); that is, close to a zonal length scale of 4100 km at that latitude. Its response function is shown in Fig. A2. But since our aim is to create a low-pass zonal wavelength filter on a sphere, and not a high-pass wavenumber filter, the cut-

a. Very-high frequencies, momentum fluxes

b. Intermediate frequencies, momentum fluxes

c. Very-high frequencies, E-vector

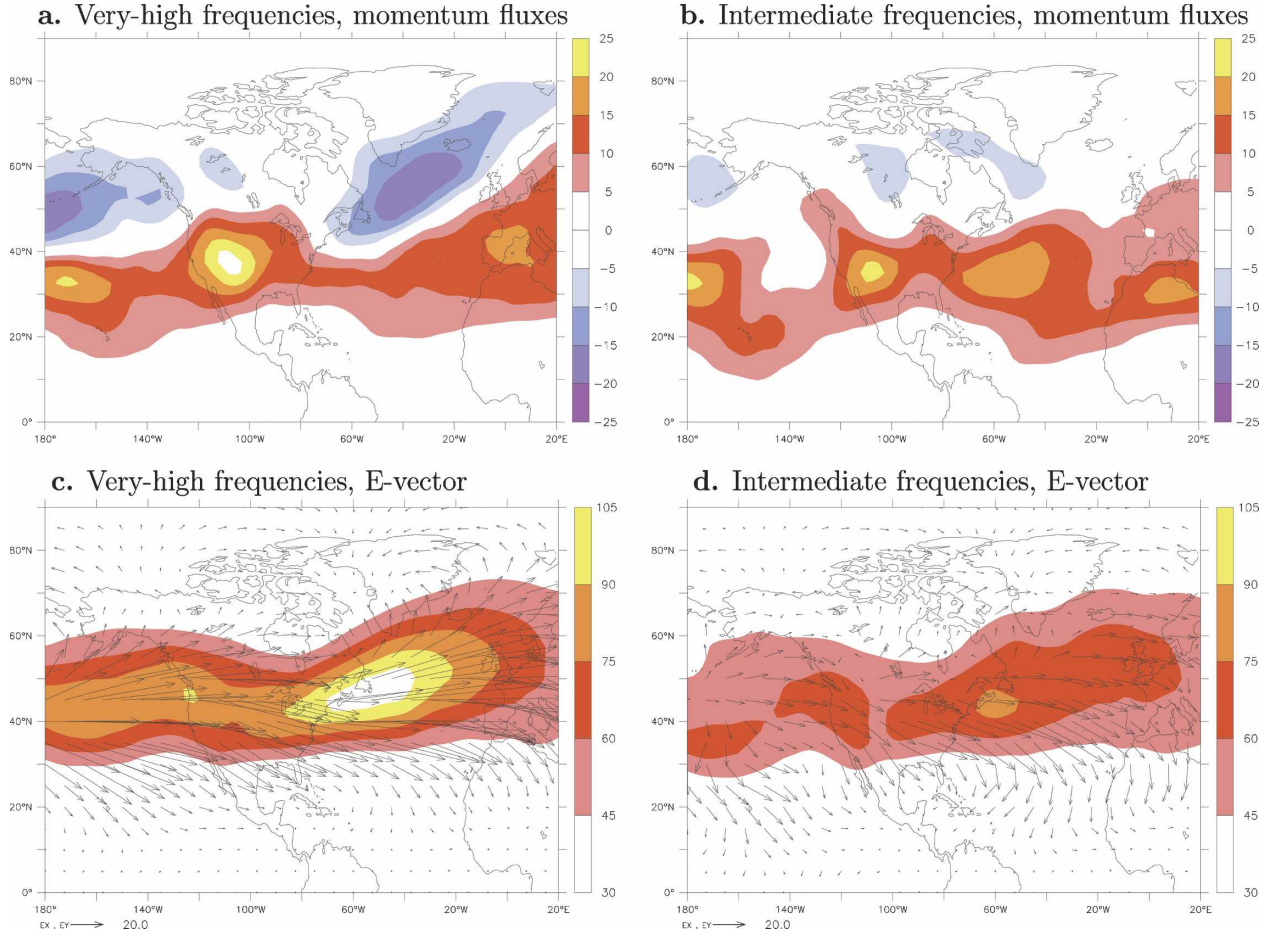**d.** Intermediate frequencies, E-vector

FIG. C1. Same as Fig. 14 but intermediate-frequency waves (periods between 5 and 12 days) and very-high-frequency waves (periods between 2 and 5 days) are directly obtained from the twice-daily dataset.

off applied at each latitude is 21 multiplied by $\cos(45°)/\cos(\varphi)$, where φ is latitude.

APPENDIX B

Regressions Representing AWB and CWB Processes

This appendix presents the exact formulation of the regressions representing AWB and CWB processes in the area A that yield to Figs. 7, 8, 9, 10, and 12. The regression corresponding to AWB processes is given by

$$\text{REG}_{\text{AWB}}(X, T) = \sum_{t \in \mathbf{P}} X(t + T) \frac{\langle u'v' \rangle_{\text{A}} - \langle u'v' \rangle_{\text{A}+}}{\text{std}_+},$$
(B1)

where X is the regressed variable, T is the time lag, $\langle u'v' \rangle_{\text{A}}$ is the average of the momentum fluxes in the area A, $\mathbf{P}$ is the ensemble of days when this average is

positive, $\langle u'v' \rangle_{\text{A}+}$ is the time average of $\langle u'v' \rangle_{\text{A}}$ when it is positive, and std_+ is the associated standard deviation. The regression associated with CWB processes can be similarly expressed as

$$\text{REG}_{\text{CWB}}(X, T) = -\sum_{t \in \mathbf{N}} X(t + T) \frac{\langle u'v' \rangle_{\text{A}} - \langle u'v' \rangle_{\text{A}-}}{\text{std}_-},$$
(B2)

where $\mathbf{N}$ is the ensemble of days when $\langle u'v' \rangle_{\text{A}}$ is negative, $\langle u'v' \rangle_{\text{A}-}$ is the time average of $\langle u'v' \rangle_{\text{A}}$ when it is negative, and std_- is the associated standard deviation. A minus sign is applied in (B2) in order to be compared with the results of (B1). For the data used in our study; that is, for days during winters from 1950 to 1999, properties of CWB and AWB processes in the area A are quite symmetric; $\mathbf{N}$ and $\mathbf{P}$ have almost the same number of days (4522 and 4548, respectively), and the time mean and standard deviation are of the same order ($\langle u'v' \rangle_{\text{A}-} = -105$, $\langle u'v' \rangle_{\text{A}+} = 96$, $\text{std}_- = 116$, and $\text{std}_+ = 107$).

APPENDIX C

Different Computations of Intermediate and Very-High-Frequency Flows

This appendix presents the difference between two different ways of computation for the intermediate and very-high-frequency flows, particularly with regard to the results shown in Fig. 14. Figure 14 is constructed as follows. We apply the 31-point filters shown in Fig. A1a to the daily average dataset to get the high-frequency flow with periods between 2 and 12 days and the very-high-frequency flow with periods between 2 and 5 days. The intermediate-frequency flow is defined as the subtraction of the high-frequency flow from the very-high-frequency flow.

Another way to get the intermediate and very-high-frequency flows is to proceed as follows. From the twice-daily dataset, we use 61-point high-pass Lanczos filters with a cutoff of 12, 5, and 2 days, respectively. This leads to flows with periods between 1 and 12 days, between 1 and 5 days and between 1 and 2 days that are called the 12-, 5-, and 2-day high-frequency flows, respectively. A new intermediate-frequency flow is defined as the difference between the 12-day and the 5-day high-frequency flows while the new very-high-frequency flow is the difference between the 5-day and 2-day high-frequency flows. The results of these new definitions are displayed in Fig. C1 and are compared with those of Fig. 14. Only slight differences are visible between the two different ways of computation; eddy energy is weaker in Fig. 14 than in Fig. C1 especially in the very-high-frequency range but this is due to the fact that a daily average not only removes the period between 1 and 2 days but also affects lower frequencies. Our conclusions are however the same if we consider Fig. 14 or Fig. C1 and shows that our results are robust and do not depend so much on how we proceed.

REFERENCES

Barnston, A. G., and R. E. Livezey, 1987: Classification, seasonality and persistence of low-frequency atmospheric circulation patterns. *Mon. Wea. Rev.,* **115,** 1083–1126.

Benedict, J. J., S. Lee, and S. B. Feldstein, 2004: Synoptic view of the North Atlantic Oscillation. *J. Atmos. Sci.,* **61,** 121–144.

Cohen, J., and M. Barlow, 2005: The NAO, the AO, the global warming: How closely related? *J. Climate,* **18,** 4498–4513.

Duchon, C. E., 1979: Lanczos filtering in one and two dimensions. *J. Appl. Meteor.,* **18,** 1016–1022.

Feldstein, S. B., 2000: The timescale, power spectra and climate noise properties of teleconnections patterns. *J. Climate,* **13,** 4430–4440.

——, 2003: The dynamics of NAO teleconnection pattern growth and decay. *Quart. J. Roy. Meteor. Soc.,* **129,** 901–924.

Franzke, C., S. Lee, and S. B. Feldstein, 2004: Is the North Atlantic Oscillation a breaking wave? *J. Atmos. Sci.,* **61,** 145–160.

Hoskins, B. J., I. N. James, and G. H. White, 1983: The shape, propagation and mean-flow interaction of large-scale weather. *J. Atmos. Sci.,* **40,** 1595–1612.

Hurrell, J. W., 1995: Decadal trends in the North Atlantic Oscillation: Regional temperatures and precipitation. *Science,* **269,** 676–679.

——, Y. Kushnir, G. Ottersen, and M. Visbeck, 2003: *The North Atlantic Oscillation: Climatic Significance and Environmental Impact. Geophys. Monogr.,* Vol. 134, Amer. Geophys. Union, 279 pp.

Kocin, P. J., and L. W. Uccellini, 1990: *Snowstorms along the Northeastern Coast of the United States: 1955 to 1985. Meteor. Monogr.,* No. 44, Amer. Meteor. Soc., 280 pp.

——, P. N. Schumacher, R. F. Morales Jr., and L. W. Uccellini, 1995: Overview of the 12–14 March 1993 superstorm. *Bull. Amer. Meteor. Soc.,* **76,** 165–182.

Lee, S., and S. B. Feldstein, 1996: Two types of wave breaking in an aquaplanet GCM. *J. Atmos. Sci.,* **53,** 842–857.

Orlanski, I., 2003: Bifurcation in eddy life cycles: Implications for storm track variability. *J. Atmos. Sci.,* **60,** 993–1023.

——, 2005: A new look at the Pacific storm track variability: Sensitivity to tropical SSTs and to upstream seeding. *J. Atmos. Sci.,* **62,** 1367–1390.

——, and J. P. Sheldon, 1995: Stages in the energetics of baroclinic systems. *Tellus,* **47A,** 605–628.

Overland, J. E., and M. Wang, 2005: The Arctic climate paradox: The recent decrease of the Arctic Oscillation. *Geophys. Res. Lett.,* **32,** L06701, doi:10.1029/2004GL021752.

Rodwell, M. J., 2003: On the predictability of North Atlantic Climate. *The North Atlantic Oscillation: Climatic Significance and Environmental Impact, Geophys. Monogr.,* Vol. 134, Amer. Geophys. Union, 173–192.

——, D. P. Rowell, and C. K. Folland, 1999: Oceanic forcing of the wintertime North Atlantic Oscillation and European climate. *Nature,* **398,** 320–323.

Shindell, D. T., R. L. Miller, G. Schmidt, and L. Pandolfo, 1999: Simulation of recent northern winter climate trends by greenhouse-gas forcing. *Nature,* **399,** 452–455.

Simmons, A. J., and B. J. Hoskins, 1980: Barotropic influences on the growth and decay of nonlinear baroclinic waves. *J. Atmos. Sci.,* **37,** 1679–1684.

Thorncroft, C. D., B. J. Hoskins, and M. E. McIntyre, 1993: Two paradigms of baroclinic-wave life-cycle behavior. *Quart. J. Roy. Meteor. Soc.,* **119,** 17–55.

Trenberth, K. E., 1986: An assessment of the impact of transient eddies on the zonal flow during a blocking episode using localized Eliassen–Palm flux diagnostics. *J. Atmos. Sci.,* **43,** 2070–2087.

Vallis, G. K., E. P. Gerber, P. J. Kushner, and B. A. Cash, 2004: A mechanism and simple dynamical model of the North Atlantic Oscillation and annular modes. *J. Atmos. Sci.,* **61,** 264–280.